

## 1. EXPLANATORY NOTES<sup>1</sup>

### Shipboard Scientific Party<sup>2</sup>

## INTRODUCTION

This chapter describes the sampling, measurement, and core description procedures and methods used during Leg 148 to help the reader understand the basis for our preliminary conclusions and to help investigators select samples for further analysis. This chapter concerns only shipboard operations and analyses described in the site reports in the Leg 148 *Proceedings of the Ocean Drilling Program Initial Reports* volume. Methods used for shore-based analysis of Leg 148 data will be detailed in the *Scientific Results* volume.

### Site Chapters

The site chapters describe drill sites, summarize operations, and present preliminary results. The sections of the site chapters were written by the following shipboard scientists, listed alphabetically:

Site Summary: Alt, Kinoshita  
Background and Objectives: Alt, Kinoshita  
Operations: Harding, Stokking  
Igneous Petrology: Bach, Brewer, Fisk, Furnes, Miyashita, McNeill  
Alteration and Metamorphism: Alt, Honnorez, Ishizuka, Laverne, Teagle, Vanko  
Aqueous Geochemistry: Bach, Magenheimer  
Igneous and Metamorphic Geochemistry: Bach, Brewer, Furnes, Honnorez, Ishizuka, Laverne, Magenheimer, Miyashita  
Structure and Deformation: Allerton, Dilek, Harper, McNeill, Tartarotti  
Paleomagnetism: Allerton, Stokking, Worm  
Physical Properties: Fujisawa, Pezard, Salisbury, Wilkens  
Downhole Measurements: Becker, Boehm, Filice, Guerin, Hoskins, Kinoshita, Pezard, Wilkens, Worm  
Lithostratigraphic Summary: Alt, Kinoshita  
Summary and Conclusions: Alt, Kinoshita  
Appendix: Shipboard Scientific Party

Summary core descriptions (visual core descriptions for igneous and metamorphic rocks), thin-section descriptions, and photographs of each core follow the text of the site chapters.

### Shipboard Scientific Procedures

#### *Numbering of Sites, Holes, Cores, and Samples*

Drill sites are numbered consecutively from the first site drilled by the *Glomar Challenger* in 1968. A site number refers to one or more holes drilled while the ship was positioned over one acoustic beacon. Multiple holes may be drilled at a single site by removing the drill pipe from the hole, repositioning the ship, and then drilling another hole. The ship may return to a previously visited site to drill additional holes, or to log or deepen a previously existing hole, as was the case with Hole 504B.

For all ODP drill sites a letter suffix distinguishes each hole drilled at the same site. For example, the first hole drilled is assigned the site number to which is added the suffix *A*, the second hole takes the site number and suffix *B*, and so forth. This procedure prevents ambiguity between site- and hole-number designations, though it differs from DSDP designations for Sites 1 through 624. Distinguishing holes drilled at a site is critical because recovered rocks from different holes usually do not come from equivalent positions in the stratigraphic column.

The cored interval is measured in meters below seafloor (mbsf); sub-bottom depths are determined by subtracting the drill pipe measurement (DPM) water depth—the length of pipe from the rig floor to the seafloor—from the total DPM, which extends from the rig floor to the bottom of the hole (Fig. 1). Water depths below sea level can be determined by subtracting the height of the rig floor above sea level from the DPM water depth. The rig-floor height varies from site to site and is given in the hole, depth, and location summary tables in each site report. Echo-sounding data from the precision depth recorders are used to locate the site, but usually are not used as a basis for any further measurements. A water depth of 3460 m, determined on previous legs by echo sounding, is used in the Leg 148 *Initial Reports* to be consistent with depths reported from previous visits to Site 504.

The depth interval assigned to an individual core begins with the depth below the seafloor at which coring began and extends to the depth at which coring ended for that core (Fig. 1). For rotary coring (RCB), each coring interval is equal to the length of the joint of drill pipe added for that interval, although a shorter core may be attempted in special instances. The drill pipe varies from approximately 9.4 to 9.8 m. The pipe is measured as it is added to the drill string, and the cored interval is recorded as the length of the pipe joint to the nearest 0.1 m.

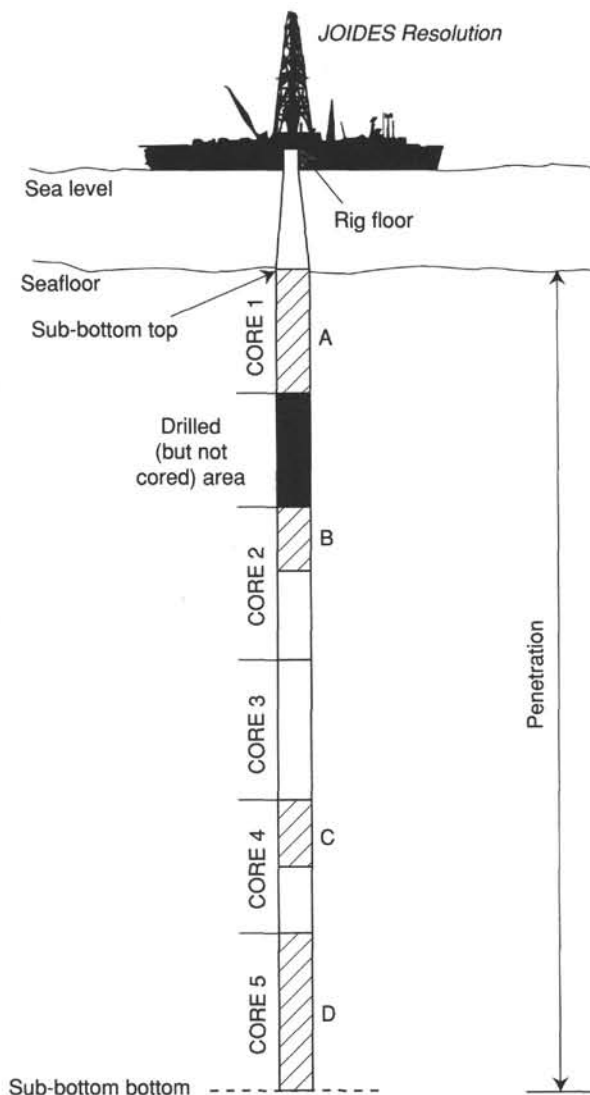
Cores taken from a hole are numbered serially from the top of the hole downward. Core numbers and their associated cored intervals (in mbsf) are unique in a given hole. Maximum full recovery for a single core is 9.5 m of rock contained in a plastic liner with a 6.6-cm internal diameter, plus about 0.2 m in the core catcher, which has no plastic liner (Fig. 2). The core catcher is a device at the bottom of the core barrel that prevents the core from sliding out as the barrel is retrieved from the hole.

Each recovered core is divided into 1.5-m sections that are numbered serially from the top (Fig. 2); individual pieces of rock are then assigned a number. Fragments of a single piece are assigned a single number, and individual fragments are identified alphabetically (Fig. 3). When full recovery is obtained, the sections are numbered from 1 through 7, with the last section possibly shorter than 1.5 m. Although it is rare, an unusually long core may require more than 7 sections. When less than full recovery is obtained, there will be only the number of sections necessary to accommodate the length of the core recovered. For example, 4 m of core would be divided into two 1.5-m sections and one 1-m section. In rare cases a section less than 1.5 m may be cut in order to preserve features of interest, such as lithological contacts. The core-catcher sample is placed at the bottom of the last section of hard-rock core and is treated as part of the last section. Scientists completing visual core descriptions describe each lithologic unit, noting core and section boundaries as physical reference points.

When the recovered core is shorter than the cored interval, as is usually the case, the top of the core is considered the top of the cored

<sup>1</sup> Alt, J.C., Kinoshita, H., Stokking, L.B., et al., 1993. *Proc. ODP, Init. Repts.*, 148: College Station, TX (Ocean Drilling Program).

<sup>2</sup> Shipboard Scientific Party is as given in the list of participants preceding the contents.



-  Represents recovered material
- BOTTOM FELT:** distance from rig floor to seafloor
- TOTAL DEPTH:** distance from rig floor to bottom of hole (sub-bottom bottom)
- PENETRATION:** distance from seafloor to bottom of hole (sub-bottom bottom)
- NUMBER OF CORES:** total of all cores recorded, including cores with no recovery
- TOTAL LENGTH OF CORED SECTION:** distance from sub-bottom top to sub-bottom bottom minus drilled (but not cored) areas in between
- TOTAL CORE RECOVERED:** = A + B + C + D (in diagram)
- CORE RECOVERY (%):** = total core recovered ÷ total length of cored section x 100

Figure 1. Diagram illustrating terms used in the discussion of coring operations and core recovery.

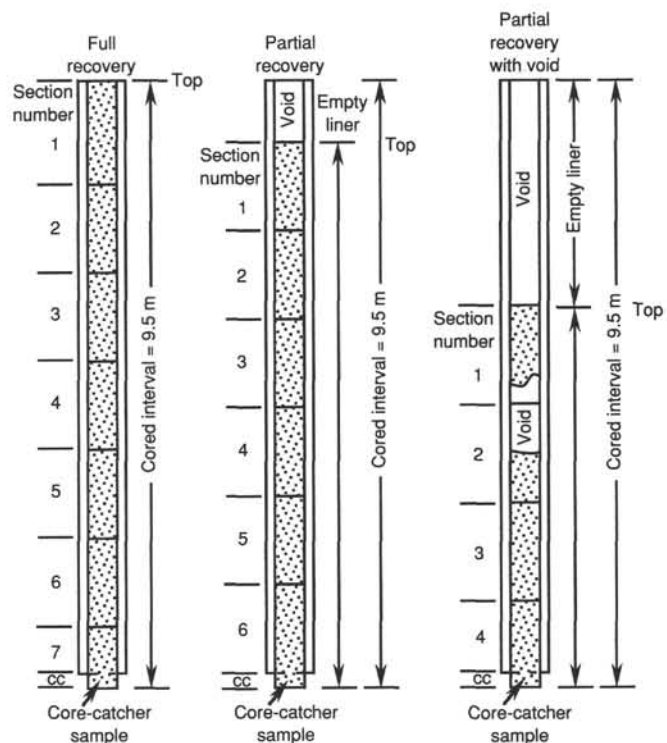


Figure 2. Diagram of procedure for cutting and labeling core sections.

interval to achieve consistency in handling analytical data derived from the cores. Samples removed from the cores are designated by distance measured in centimeters from the top and bottom of each sample removed from that section. In curated hard-rock sections, sturdy plastic spacers are placed between pieces that do not fit together to maintain the order of the pieces and to protect them from damage in transit and in storage. Thus, the centimeter interval noted for a hard rock sample has no direct relationship to that sample's depth within the cored interval and is only a physical reference to the location of the sample within the curated core.

The identification number for a sample consists of the leg, site, and hole designation, the core number, core type, section number, piece number (for hard rock), and interval measured in centimeters from the top of section. For example, Sample 148-504B-186R-1, 10–12 cm, represents a sample removed from the interval between 10 and 12 cm below the top of Section 1, Core 186 (R designates that this core was taken during rotary coring) from Hole 504B during Leg 148.

All ODP core and sample identifiers indicate core type. The following abbreviations are used: R = Rotary Core Barrel (RCB); B = drill-bit recovery; I = in-situ water sample; W = wash-core recovery; and M = miscellaneous material. R and M cores were cut on Leg 148.

### Core Handling

#### Igneous Rocks

Igneous rock cores are handled differently from sedimentary cores. Once on deck, the core catcher is placed at the bottom of the core liner, and total core recovery is calculated by shunting the rock pieces together and measuring to the nearest centimeter; this information is logged into the shipboard core-log database. The core is then cut into 1.5-m-long sections and transferred to the lab. The contents of each section are transferred into 1.5-m-long sections of split core liner, where the bottoms of oriented pieces (i.e., pieces that clearly could not have rotated top to bottom about a horizontal axis in the liner) are

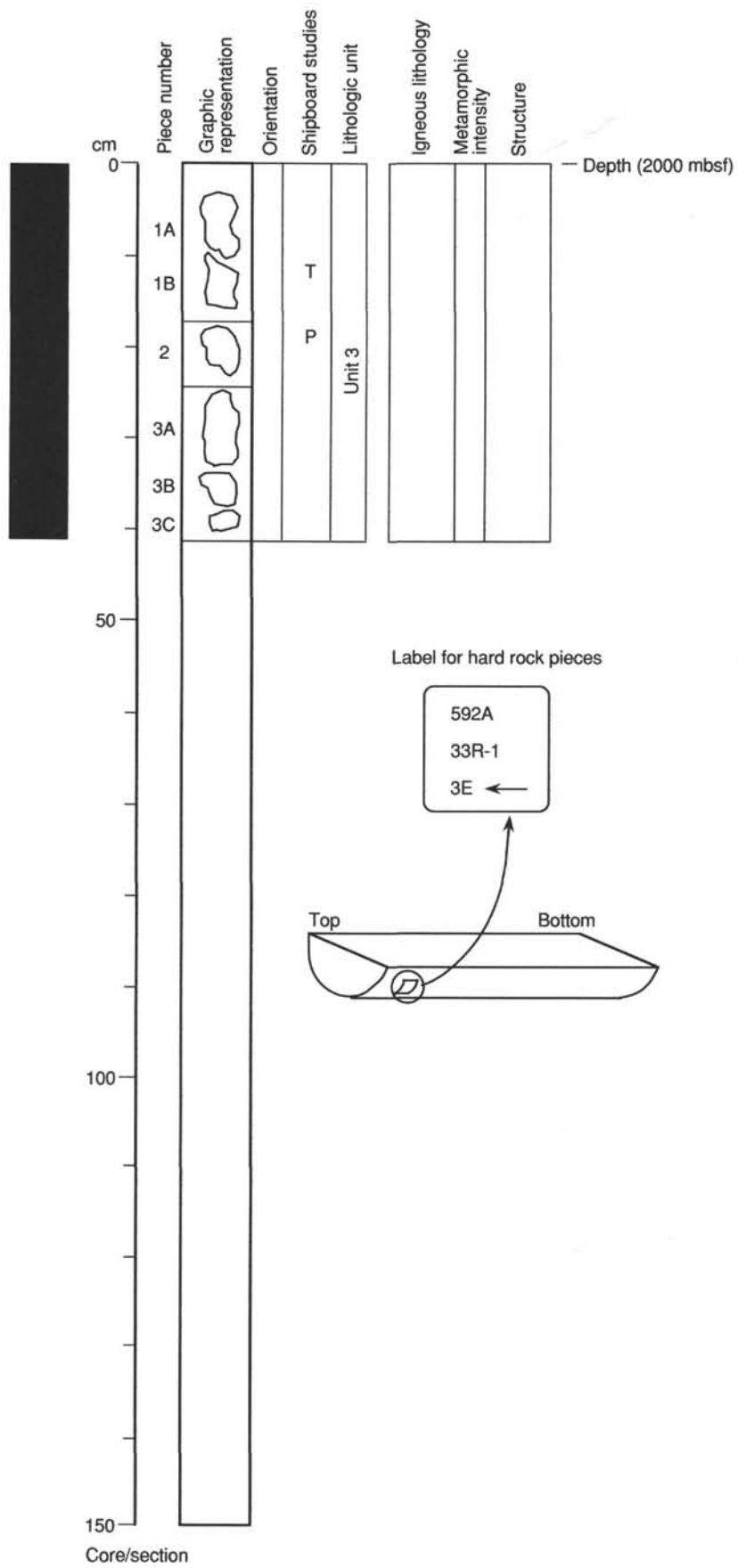


Figure 3. Numbering system for hard-rock pieces.

marked with a red wax pencil. This is to ensure that orientation is not lost during the splitting and labeling process. To facilitate structural observations and measurements, a structural geologist marks each piece for splitting so that the principal structure dips parallel to the cut. The core is then split with a diamond saw into archive and working halves, and plastic spacers are inserted between pieces. Each piece is numbered sequentially from the top of each section, beginning with number 1. Reconstructed groups of pieces are assigned the same number, but are lettered consecutively (i.e., 1A, 1B, 1C, etc.). Pieces are labeled only on external surfaces. If the piece is oriented, an arrow is added to the label pointing to the top of the section.

The archive half is depicted on the hard-rock visual core description form, noting size, shape, orientation, and special features of each piece (see "Visual Core Description" section, this chapter). Most archive sections longer than 20 cm are run through the cryogenic magnetometer. The archive half is then photographed in both black-and-white and color. The shipboard scientific party may request black-and-white close-up photographs of particular features for illustrations in each site summary.

The archive halves of Leg 148 cores were described by igneous petrologists, metamorphic petrologists, and structural geologists. After the cores were described on Leg 148 aboard ship, the working halves were sampled for shipboard thin sections, physical properties, magnetic studies, X-ray fluorescence (XRF), and carbon-hydrogen-nitrogen-sulfur analyses. Analytical methods are described later in this chapter and the data are reported in the site chapter. Representative samples were taken from each lithologic unit for XRF analyses of major and selected trace elements whenever possible. Near the end of Leg 148, samples were taken from the working halves for shore-based laboratory studies. Each extracted sample was logged into the computer database by the location of the sample within the curated core and the name of the investigator receiving the sample. The extracted samples are sealed in plastic vials or bags and labeled. The curator at ODP keeps records of all samples.

Both halves of the core are then shrink-wrapped in plastic to prevent rock pieces from vibrating out of sequence during transit, put into labeled plastic tubes, sealed, and transferred to cold-storage space aboard the ship. All Leg 148 cores are housed in the Gulf Coast Repository.

## OPERATIONS

### Drilling Systems

The rotary core barrel (RCB) coring system (Fig. 4) used during Leg 148 has been the primary rock-recovery tool of DSDP and ODP. The RCB system's inner core barrels are wireline-retrievable, in contrast to the oil-field coring version. A special high-speed winch and 0.5-in. wire rope are used to retrieve the inner core barrel for each core, eliminating the need to trip the drill string. The coring system type is determined by the nature of the material cored. The RCB system can obtain representative core samples from many kinds of sediment or rock, and it is the only known system that can core an entire sediment column a kilometer or longer and then core crystalline basement rocks without a bit change. The core is trimmed by the rotating cones of a roller-cone bit before passing through the rotating bit throat and entering the non-rotating inner core barrel. The core barrel and its plastic liner are decoupled from drill-string rotation by bearings at top and bottom. The cored interval is determined by the length of pipe added.

The bits used with the RCB system have 4 roller cones. The RCB bit diameter is 9-7/8 in. to 10-1/8 in., and the core throat diameter is 2-7/16 in. Because of the small opening and the use of a flapper-type check valve above the bit, the bit must be dropped by using a mechanical bit release (MBR) before most logging or other tools can pass out of the drill string (see "Downhole Measurements" section, this chapter). RCB bits employ a variety of tungsten-carbide cutting structures, depending upon anticipated lithology. Longer chisel-shaped inserts

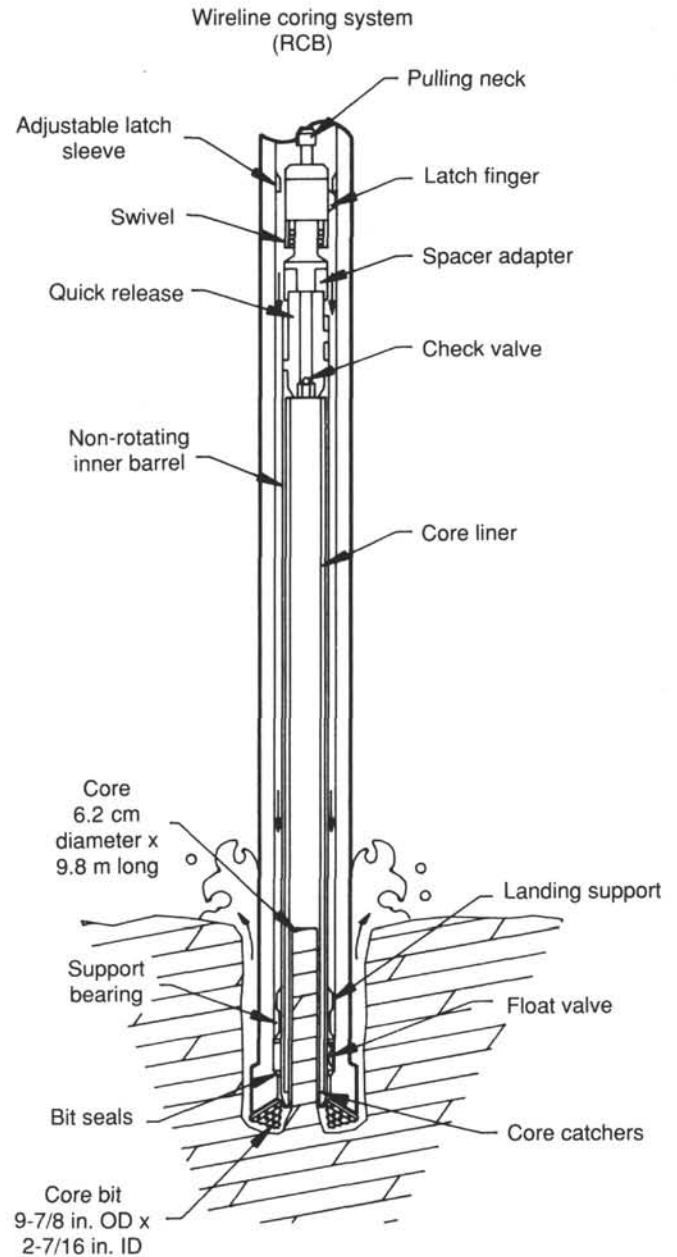


Figure 4. Rotary core barrel (RCB) coring system.

are used for gouging soft-to-medium material, whereas shorter chisel- or conical-shaped inserts are used for drilling in high-compressive-strength rocks through point loading. Medium-length chisel inserts are used where lithology is varied or unknown. RCB bits specially hardened to increase rotating time from 15 to 20–30 hr per bit were used for Leg 148 operations.

### Drilling Characteristics

#### Drilling Parameters

Because water circulation in the borehole is open, cuttings are lost and cannot be examined. Information concerning lithologic stratification in uncored or unrecovered intervals may be inferred from seismic data, wireline-logging results, and from an examination of the behavior of the drill string as observed and recorded on the drilling platform. Typically, harder layers are more difficult to penetrate. The

driller must vary the weight on bit (WOB), rotations per minute (rpm), and circulation rate parameters to optimize core recovery and rate of penetration (ROP). WOB may range from 5000 lb in soft, shallow sediments to 40,000 lb in crystalline rocks and depends upon the type of material being penetrated, the kind of bit in use, and the amount of drill-collar weight that can be applied to the bit. The drill string is rotated at 35–100 rpm, again depending on the type of bit and the nature of the formation.

The driller monitors rotary torque and circulating pressure to determine downhole conditions. An increase in the torque required to rotate the drill string may signal hole-cleaning problems, bit failure, or severe hole deviation. The fluid circulating pressure required is determined primarily by the length of the drill string and the amount of restriction at the bit. Changes in pressure may signal successful (or unsuccessful) latch-in of the inner barrel at the bit, hole-cleaning problems, or plugged bit nozzles.

The above parameters are recorded in analog form by the Martin-Decker drilling recorder on the drill floor; the records are available from ODP Engineering and Drilling Operations. A computerized TOTCO drilling recorder system that will digitally record drilling data is being developed.

### Drilling Deformation in Rotary Cores

#### *Grooving*

Core-catcher teeth, or “dogs,” often cause longitudinal or spiral external marks on the cores. Longitudinal marks may result from rock chips or debris behind one or more of the core-catcher dogs. Often, and for unknown reasons, the RCB core barrel does not remain stationary with respect to the core but instead rotates with the outer barrel. This rotation results in lathe-machining type spiral grooving caused by the core-catcher dogs and can severely reduce core diameter.

#### *Fracturing, Disintegration, and Discing*

The proportion of core fracturing that results from drilling and coring processes is not known. Sometimes cores are recovered so severely fractured and broken that they fall apart when the liners are split. In some cases the brittle failure of the core can be related to open fractures, strong veining, and/or paleotectonic textures. However, at greater depths core discing, which does not correspond to fractures, veins, or textures, is obvious. Discing breaks are perpendicular to the hole axis, and disk morphology is often buckled and saddle-shaped, with thicknesses of 1–10 cm. Different zones of stress concentration at the bottom of the borehole lead to core failure during drilling. Core discing, in-situ stress, and rock mechanical properties of the rocks are probably correlated. Core discing occurred frequently in Leg 148 cores and is described in the Site 504 chapter.

## VISUAL CORE DESCRIPTION

### Hard-rock Core Description

Observations of hard rocks were recorded on Visual Core Description Igneous/Metamorphic (VCD) forms and were tabulated in additional logs described below. The archive half of each core was drawn in the left column of the VCD, noting size, shape, orientation, and special features of each piece. A horizontal line across the entire width of the drawing denoted a plastic spacer glued between rock pieces inside the liner. Oriented pieces were indicated on the form by an upward-pointing arrow to the right of the piece. The depth (in mbsf) of the top of each section was indicated on each VCD. The archive half of each core was photographed in both black-and-white and color, and close-up photographs (black-and-white) were taken of particular features for illustrations as requested by the shipboard scientific party.

The archive core halves were described by igneous, metamorphic, and structural geologists, who generated separate core description logs (see the “Igneous Petrology,” “Alteration and Metamorphism,”

and “Structure and Deformation” sections of this chapter). To ensure uniformity of observations, a single individual was responsible for the same observations for every core. The core was divided into igneous, metamorphic, and structural units, the boundaries of which did not necessarily coincide; only the igneous units are indicated on the VCD. Shipboard samples and studies were indicated on the VCD in the column headed “Shipboard Studies” using the following notation: X = X-ray fluorescence analysis; D = X-ray diffraction; T = petrographic thin section; M = paleomagnetic analysis; and P = physical properties analysis. Analytical methods are described later in this chapter.

## IGNEOUS PETROLOGY

Lithologic units were identified based on the presence of contacts, primary mineralogy, grain size, and texture. The boundaries of the lithologic units were drawn on the VCD, and for Hole 504B the units were numbered continuously from the end of Leg 140, starting with Unit 270. For Hole 896A the unit numbers start at 1 in Core 148-896A-1R at 195.1 mbsf (approximately 15 m into basement). The igneous team described primary mineralogy, texture, structure, nature of contacts, and color for each unit. This information was recorded on three database spreadsheets and was entered into the ODP database with the program HARVI. For Hole 504B, structures were indicated in the Structure column of the VCD using symbols from Figure 5. A rock name was given to each unit based on igneous characteristics using the conventions described in the section “Rock Names.” Rock type was indicated by a pattern (Fig. 5) in the Igneous Lithology column of the VCD. For Hole 504B only basalt and diabase rock types were indicated. In Hole 896A all rocks were basalts, and patterns in the lithology column indicate whether they are pillowed, massive, or brecciated.

### Igneous Petrology Logs

The Igneous Contacts Log lists the location and type of contacts that define lithologic units. The location of the contact was recorded by core, section, position (in centimeters), and piece number, and the overlying unit number and rock name are given. When a contact was not recovered but a change of lithology was observed, a contact was indicated at the base of the lowest piece in the overlying lithologic unit. The rock name was based on the Igneous Lithology Log (see below). The character of the contact, as described in Figure 6, was listed along with a brief description of the contact, such as sharp, gradational, sutured, chilled, planar, or irregular. The dip of contacts within the diabase at Hole 504B was recorded when possible, and additional explanation was given when necessary.

The Igneous Lithology Log lists the core, section, pieces, cm interval, and unit number, as defined by the contacts and changes in lithology. Lithology (rock name), igneous textures, and color were also recorded. Details on textural descriptions are given in the “Igneous Textures” section. Color was determined by matching the dry, cut surface of the rock to the Munsell color chart. Some rocks exhibit a range of colors.

Two Igneous Mineralogy Logs were used: one for the dikes of Hole 504B, and one for the basalts of Hole 896A. Both logs include the core, section, pieces, and cm interval for each unit as given in the Igneous Lithology Log. For the dikes the phenocryst and groundmass abundance, average grain size, and grain morphology were estimated for plagioclase, pyroxene, and olivine. For euhedral and subhedral minerals the shape was further defined as equant, tabular, lath, etc. (Fig. 7). A hyphen (-) was entered to indicate the absence of a phase. If both phenocryst and groundmass morphology were described, the phenocryst morphology appears first. (The term groundmass refers to intergranular material in diabase.) Morphological terms are given in Table 1. Percent oxide minerals (% Ox) and percent sulfide minerals (% S) are estimates based on the abundance of grains greater than 50  $\mu\text{m}$  observed in hand specimen with the binocular microscope.

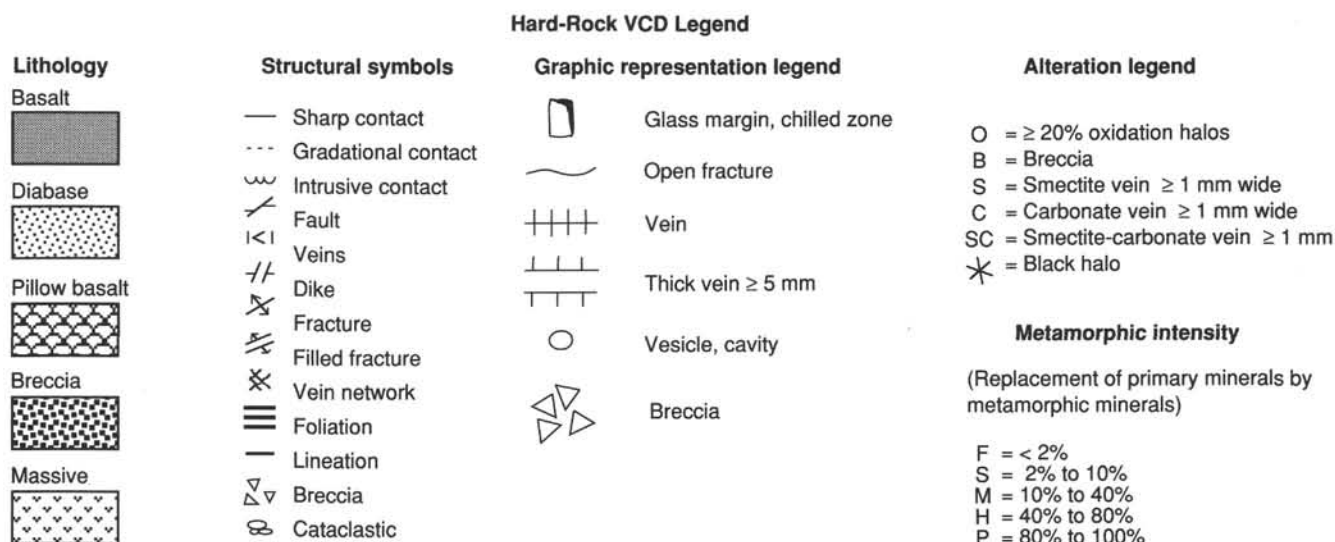


Figure 5. Hard-rock legend with patterns for the lithologies, symbols for structures and graphic representation, and codes for alteration. Two lithologies, basalt and diabase, were used for Hole 504B. Basalt from Hole 896A was divided into three lithologies: pillow basalt, breccia, and massive. The alteration legend was used to describe basalts from Hole 896A. The metamorphic intensity was applied to diabase from Hole 504B.

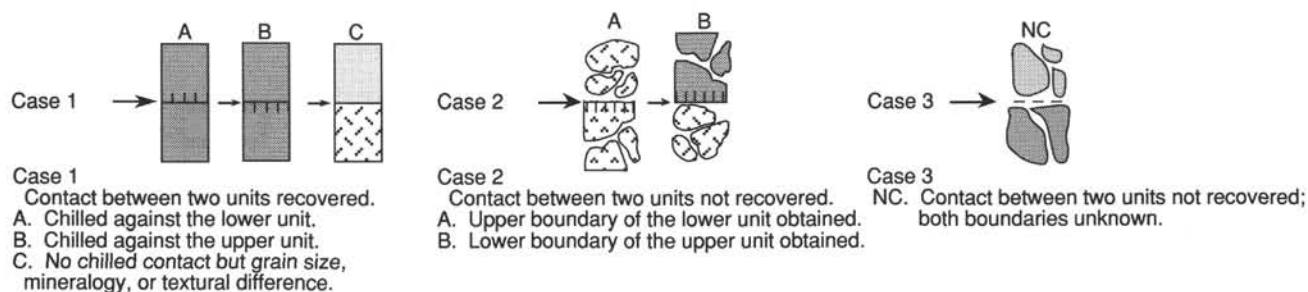


Figure 6. Types of igneous contacts.

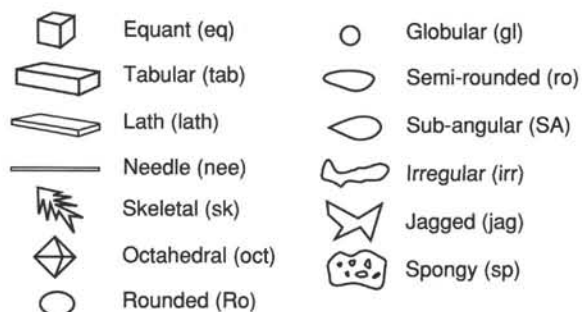


Figure 7. Atlas of crystal forms for igneous minerals.

### Igneous Textures

All of the rocks contained phenocrysts and were therefore inequigranular. Some rocks were described as seriate (crystals of the principal minerals in a continuous range of sizes); porphyritic (relatively large crystals surrounded by finer-grained groundmass); glomerophytic (a porphyritic texture of phenocrysts clustered in aggregates); poikilitic (relatively large crystals of one mineral [oikocryst] enclosing numerous smaller crystals of one or more other minerals [chadacrysts]); ophitic/subophitic (a poikilitic texture in which the randomly arranged chadacrysts are elongated and wholly or partly enclosed by the oikocryst) or intergranular (spaces between plagioclase laths occupied by one or more grains of pyroxene ± olivine and opaque minerals). These textures are summarized in Table 2.

### Igneous Structure

The Mineralogy Log for the basalts from Hole 896A was similar to the log used for the diabase from Hole 504B. However, the abundance, size, type, and shape of groundmass minerals was not estimated. The range of phenocryst abundance within each unit was also indicated. The presence of spinel or vesicles was noted.

The rock name for each unit was derived from the mineralogy using the criteria described in the "Rock Names" section of this chapter, and was recorded on all three logs. Data was extracted from these logs and entered into the ODP database with the program HARVI.

The structure of the diabase was uniformly massive and homogeneous. Three basaltic structures from Hole 896A were recognized: pillow, breccia, and massive. Pillow basalts were identified by their chilled margins, or in the absence of these margins by variolitic texture, curved fractures, microcrystalline grain-size, and radiating (columnar) cracks. Massive units were identified as fine-grained without evidence of chilled margins or other features of pillows. These massive rocks are thought to be flows or perhaps intrusions within the pillow lavas, but it is possible that some rocks identified as massive are the interiors

**Table 1. Individual mineral morphology.**

Individual mineral morphologies and characteristics with abbreviations
1. Phenocryst
A. Anhedral (an)
B. Subhedral (su)
C. Euhedral (eu)
D. Twinned (tw)
E. Mineral inclusions (in)
F. Reaction rim or corona (rr)
G. Skeletal (sk)
H. Pseudomorph (ps)
2. Microphenocryst
3. Subophitic
4. Ophitic
5. Oikocryst
6. Chadacryst
7. Cumulus crystal
8. Intercumulus crystal
9. Crescumulus crystal

**Table 2. Rock textures.**

Rock texture
1. Aphanitic
A. Microcrystalline
B. Cryptocrystalline
C. Glassy
2. Phaneritic
A. Fine-grained
B. Medium-grained
C. Coarse-grained
3. Equigranular
A. Panidiomorphic granular
B. Hypidiomorphic granular
C. Allotriomorphic granular
4. Inequigranular
A. Seriate
B. Porphyritic
C. Glomerophyric
D. Poikilitic
E. Ophitic/subophitic
F. Intergranular
5. Varitextured
6. Cumulate
A. Orthocumulate
B. Mesocumulate
C. Adcumulate
7. No texture determined

of large pillow basalts whose rims were not recovered. Pillow basalts were fragile and possibly less easily recovered, resulting in under representation relative to massive rocks at Hole 896A.

### Rock Names

The igneous rocks were named according to the abundance of primary minerals. As in Leg 140 the majority of the rocks recovered at Hole 504B are holocrystalline, fine-grained rocks, and the root word "diabase" has been used for these rocks. At Hole 896A almost all of the rocks have groundmass mineralogy too fine grained to be identified in hand specimen and are called basalts.

Diabase and basalts were described as aphyric (<1%), sparsely phyric (1%–2%), moderately phyric (2%–10%), or highly phyric (>10%), depending upon the proportion of phenocrysts. They were further classified by the types of phenocrysts or megascopic crystals

present (e.g., moderately plagioclase-olivine phyric, in which the amount of plagioclase exceeds the amount of olivine).

Leg 140 abbreviations for these rock names have been adopted for Leg 148: P, O, C, OP, OPC, and A, where P = plagioclase, O = olivine, C = clinopyroxene, and A = aphyric. On Leg 148, however, phenocryst phases were listed in order of abundance, adding the additional categories PO, OC, CP, POC, OCP, COP, and CPO. When a mineral made up less than 0.5% of the rock, the mineral was not included in the name. Similar naming conventions were used on Legs 69, 70, 83, 111, and 137 and are outlined in the Leg 140 *Initial Reports* volume (Dick, Erzinger, Stokking, et al., 1992, p.52).

### HARVI Database

The Igneous Contacts, Lithology, and Mineralogy Logs are presented as appendixes, and summary descriptions of each rock unit are given in the Core Descriptions at the end of the volume. To ensure consistency with previous studies, data from the igneous logs were entered into the HARVI database. Each record is printed in a format that can be directly pasted onto the barrel sheet for curatorial handling. The following information was recorded in the HARVI database system for each lithologic unit and section:

1. The leg, site, hole, core number, core type, and section number.
2. The unit number (consecutive down-hole), position in the section, number of pieces of the same lithologic type, the rock name, and the identification of the observer (on Leg 148, IMS was used to indicate that each unit was described by the igneous, metamorphic, and structural teams).
3. The Munsell color number of the dry rock and the presence and character of any structural fabric.
4. The number of mineral phases visible with a hand lens and mineral phase distribution within the unit, with the following information for each phase: abundance (volume percent), size range in millimeters, shape (anhedral, subhedral, or euhedral), degree of alteration, and further comments if appropriate.
5. The groundmass texture: glassy, equigranular, fine-grained (<1 mm), medium-grained (>1 mm and < 5 mm), or coarse grained (> 5 mm). Grain-size changes within units were also noted.
6. The presence and characteristics of secondary minerals and alteration products.
7. The abundance, distribution, size, shape, and infilling material of vesicles, including the proportion of vesicles that are filled by alteration minerals.
8. The intensity of metamorphism, expressed as a percentage of primary phases replaced by secondary minerals: fresh (<2%), slightly metamorphosed (2%–10%), moderately metamorphosed (10%–40%), highly metamorphosed (40%–80%), and pervasive (80%–100%). This scale is represented in the metamorphic intensity column on the VCD forms by the letters F, S, M, H, and P, respectively.
9. The presence of veins and fractures, including their abundance, width, mineral fillings or coatings, and orientation.
10. The presence of structural features, including the orientation of igneous contacts, igneous layering, magmatic fabrics, cataclastic features, fractures, and faults.
11. Other comments, including notes on the continuity of the unit within the core and on the interrelationship of units.

### Thin Sections

Thin sections of igneous rocks were examined to complement and refine the hand-specimen observations. These observations included noting textural features that were not identified in hand specimen, precise determination of grain size of phenocrysts and groundmass, the type and intensity of mineral zoning, the mineralogy and abundance of glomerocrysts, the presence of inclusions within phenocrysts, and the presence of spinel. Diabase and basalt were described

differently because most basalts had groundmass too fine grained for the mineralogy and grain size to be determined.

The abundance of each mineral phase was determined by counting 500 points using an automatically advancing stage with an attached counter. Primary mineral abundances were counted, with pseudomorphs counted as their primary precursors. In some of the rocks plagioclase and augite were seriate porphyritic so phenocrysts and groundmass were not easily distinguished.

Crystal sizes of all primary phases were measured. For plagioclase, olivine, and pyroxene a representative area of the section was selected and minerals within that area were measured along their longest axis. In Hole 896A, 100 grains were measured in one thin section from each unit. The range of lengths was recorded. For plagioclase and magnetite in Hole 504B the width and length of 100 grains was measured in each thin section and the diameter of a circle with equivalent area calculated. This diameter was recorded as the size of the grains. Magnetite grain size was determined in the same way, but in Hole 896A they were not measured because of their small size.

In addition to abundances, mineral morphologies, and grain sizes, textural features were described. In the dikes (Hole 504B) the terms subophitic, ophitic, or intergranular were used to describe the mesostasis (MacKenzie et al., 1982), and the terms porphyritic and glomerophytic were used to indicate whether the phenocrysts occurred as single grains or as clusters. All the dikes had an average grain size of less than 1 mm and were termed fine-grained. Additional textural terms were used for the basalts (Hole 896A). Glomerophytic and porphyritic were used to describe the phenocrysts as for the dikes, and when both terms were used the first one indicated the dominant form of phenocrysts. The groundmass texture was described as radiate, intersertal, intergranular, or subophitic (MacKenzie et al., 1982). The terms used for the grain size of the groundmass were fine-grained, microcrystalline, cryptocrystalline, and glass. In fine-grained rocks the groundmass mineralogy could be identified; in microcrystalline rocks the crystals could be seen but not identified; in cryptocrystalline rocks the crystals could not be seen; glass indicates no crystals. When more than one grain size applied to a rock, the term for the dominant texture was placed first.

Descriptions of mineral inclusions, "xenocrysts" and "xenoliths," and the zoning within minerals were included in the comment section of the Thin-Section Description Form. This information was recorded in the computerized database HRTHIN. The same terminology used for thin-section descriptions was used for the megascopic descriptions (see Tables 1 and 2). Thin-section descriptions are included in the appendixes and are also available from the ODP database.

## ALTERATION AND METAMORPHISM

Alteration and metamorphic visual core descriptions were conducted following documentation of the core by the igneous working group. Alteration and vein visual core description logs were used to provide consistent and complete characterization of the core, and a subset of the data was entered into the HARVI database. To ensure accurate core descriptions, thin-section petrography was integrated with visual core descriptions where possible. The alteration and vein logs include documentation of alteration, mineralogy and petrology, and definition of alteration units. The alteration logs for Holes 504B and 896A (Appendixes G, "Site 504" chapter, and E, "Site 896" chapter, this volume) describe secondary mineralogy and secondary features such as veins and alteration halos. The log used for Hole 896A is modified slightly from the one used for Hole 504B, owing to the different styles of groundmass alteration and other differences observed in the two cores.

Abbreviations for lithology, color, and mineralogy terms used in the alteration and vein logs are listed in Table 3. For rock descriptions, the core was examined for different alteration units on the basis of changes in secondary mineral occurrence and abundance in both rocks and veins, as well as texture, grain size, rock composition, and presence

**Table 3. Abbreviations related to lithology, alteration, and veins.**

Abbreviation	Term
<b>Lithology</b>	
db	diabase
<b>Color</b>	
gm	green
lt	light
dk	dark
med	medium
brn	brown
w	white
pistach	pistachio
clrlss	colorless
<b>Mineralogy</b>	
clay	undifferentiated clay minerals
cp	chalcopyrite
cpx	clinopyroxene
ab	albite
act	actinolite
an	anorthite
ap	apatite
cc	calcite
carb	undifferentiated carbonate
chl	chlorite
ep	epidote
Fe hyd	undifferentiated iron oxy-hydroxides
iddings	iddingsite
ilm	ilmenite
mt	magnetite
preh	prehnite
py	pyrite
qtz	quartz
smect	smectite
tt	titanite
zco	zeolite
<b>Other abbreviations</b>	
g'mass	groundmass
Oxid.	oxidation
AW	average width (mm)
Orient	orientation
AZ	azimuth
Alt	alteration
W	halo width (mm)
%h	abundance of halos as percentage of halos per piece

and type of breccias. Such alteration units could overlap or crosscut lithologic units defined by igneous features. For each unit and section, the following information was recorded in the log database:

1. The leg, site, hole, core number, core type, section number, piece number (consecutive downhole), length of the piece or pieces being described, and position in the section were recorded in the alteration and vein log sheets. Lithologies were recorded in the alteration databases. Each log has a final column for specific comments.

The following information was recorded in the individual databases:

2. Alteration Log. The alteration logs were used to describe rocks with a clear igneous protolith. The data recorded include the mineralogy and degree of alteration (visual volume-percent estimate) of each primary phenocryst type and of the igneous groundmass. Volume estimates were verified where possible by point-counting thin sections. Characterization of amygdules and related alteration halos includes their size (a length scale), an estimate of the total percent of the host rock represented by amygdules and halos, and the mineralogy of vug-filling minerals and mineral phases defining the halos. In the Hole 896A log, visual estimates of the volume percent of variously colored groundmass alteration (e.g., gray, red, yellow) are recorded for each piece of the core.

3. Vein Log. Veins were referenced on the vein log in centimeters below the top of each section. Vein type was based on color and/or mineralogy, width, orientation, and vein abundance expressed as the volume percent of the enclosing piece (Appendixes H, "Site 504" chapter, and F, "Site 896" chapter, this volume). Documentation of

vein-related alteration halos includes halo type (based on color), abundance of secondary phases comprising the halo, halo half-width, and abundance of halos expressed as the percentage of the piece represented by the halo.

## BOREHOLE FLUID GEOCHEMISTRY

### Sampling Operations

Samples were obtained using the flow-through borehole fluid sampler provided by the Los Alamos National Laboratories and described in detail in the Leg 137 *Initial Reports* (Becker, Foss, et al., 1992). Two samplers of the same design were used: one constructed of stainless steel (1.000 L), and one of titanium (0.987 L). The samplers are deployed in the open position, allowing water to flow through the sample chamber as it is lowered into the borehole. A clock activates a trigger that closes the sampler at a specific time. The samplers were run one at a time in the coring line on a sampling schedule designed to optimize time allotted for water sampling and not disturb the borehole water column for subsequent samples. Sampling was conducted from shallow to deeper depths to minimize disturbing the water deeper in the borehole column. During Leg 137 it was apparent that running the sampler too fast in the borehole resulted in poor samples. For this reason we limited in-hole speed to 50 m/min or less. The samplers were lowered to 400 m above the intended sample depth and slowed to 20 m/min, then slowed to 10 m/min at 200 m above the sampling depth. Over the last 50 m above the intended depth the samplers were slowed to a stop. The samplers were then held at depth for at least 20 min to guarantee sufficient time for the clocks to activate the trigger. The samplers were then withdrawn from the borehole at a maximum rate of 50 m/min.

### Sample Extraction Procedure

Fluid samples were removed from the samplers within 30 min of arrival on deck. Sample extraction was performed as on Leg 137, with some modification. Preventing sample contact with oxygen prior to preservation was a primary concern during sample removal because iron hydroxides have been observed to precipitate rapidly from Hole 504B borehole samples in the past. The sampler was placed in a semi-vertical position, and two valve pushers were connected to the samplers. The samples were removed through the bottom valve by pushing the samples out with a stream of nitrogen gas from the top. All extraction instruments were flushed with nitrogen prior to contact with the sample. Sub-samples were taken for various shipboard and shorebased purposes.

Sample aliquots are described in the order they were taken, in Table 4. First, a small quantity (<60 mL) was withdrawn directly into a plastic bottle to remove most of the settled particulate material. The sampling line was connected to a Cu tube for shorebased dissolved-gas and isotopic studies. At least 100 mL was flushed through the Cu tube to obtain a smooth, bubble-free stream. The overflow was collected in a 500-mL glass bottle for analysis of tritium. The Cu tube was sealed with refrigerator clamps, and another tube was filled by the same procedure. After the Cu tubes were filled and 500 mL was collected for tritium analysis, the sample stream was run into a nitrogen-filled glove bag. A pre-cleaned 0.45- $\mu$ m cellulose-acetate membrane filter was then attached for filtering all subsequent samples. Aliquots were then placed in bottles to which preservation reagent had been added. Two 15-mL bottles containing 15  $\mu$ L of a 1 M CdNO<sub>3</sub> were filled to trap sulfide for shipboard sulfide analysis and shorebased sulfur-isotopic analyses. Samples were placed in bottles containing HCl and HNO<sub>3</sub> for shipboard and shorebased investigations. Use of the glove bag with immediate preservation allows the samples to be fixed prior to any exposure to atmospheric oxygen, essentially eliminating the possibility of precipitation of iron hydroxides that can co-precipitate other elements of interest.

**Table 4. Division of borehole fluid samples (listed in chronological order).**

Aliquot no.	Quantity/Container	Function
1	60 mL muddy H <sub>2</sub> O/Poly bottle	Mineralogical observations
2	2–15 mL/Cu tubes	Dissolved gases/ He isotopes
3	500 mL/Glass bottle	Tritium analysis
4	2–23 mL/Glass septum vials	CO <sub>2</sub> (shipboard)/ $\delta$ D, $\delta^{13}$ C
5	2–15 mL/Poly with CdNO <sub>3</sub>	H <sub>2</sub> S (shipboard)/ $\delta$ D, $\delta^{34}$ S
6	30 mL/Poly	Shipboard untreated
7	100 mL/Poly with HCl	Shipboard/shorebased trace analyses
8	250 mL/Poly with HNO <sub>3</sub>	Shorebased/REE, trace analyses

Note: All fluid samples including and after aliquot 4 were filtered with an in-line 0.45- $\mu$ m cellulose acetate filter and processed in a nitrogen-filled glove bag.

### Identifying Large-volume Borehole Fluid Samples

Borehole water sample depths are unrelated to core depths because water sampling usually takes place after the borehole is drilled. For this reason we have not assigned depth-related core identifiers to each water sample. The curatorial and analytical data for these samples are in a separate water-chemistry database at ODP; these data, as are all other ODP data, are available to researchers by request.

Identifiers for borehole water samples are keyed accordingly: the first letter of the identifier, *B*, designates that it is a borehole sample; the second letter indicates the type of sampler used, either *S* for the stainless steel sampler from Los Alamos National Lab, or *T* for the titanium sampler from Los Alamos National Lab. The following list gives the codes used for the sampler runs:

- BS-1M Los Alamos Lab (LANL) sampler, on the wireline (sample lost)
- BT-2M Los Alamos Lab (LANL) sampler, on the wireline
- BS-3M Los Alamos Lab (LANL) sampler, on the wireline
- BT-4M Los Alamos Lab (LANL) sampler, on the wireline
- BS-5M Los Alamos Lab (LANL) sampler, on the wireline
- BT-6M Los Alamos Lab (LANL) sampler, on the wireline
- BS-7M Los Alamos Lab (LANL) sampler, on the wireline (sample lost)
- BT-8M Los Alamos Lab (LANL) sampler, on the wireline

Third (and fourth) letters indicate the purpose for which a subsample was taken; the addition of these letters moves the run number to the position of core number in the identifier. For example, from each sample an aliquot was taken from an acidified subsample to be returned to the Gulf Coast Repository; its designation is BSPA, indicating that it was acidified and stored in plastic.

### Analytical Methods

Borehole fluid samples and local surface seawater were analyzed for pH, alkalinity, salinity, sulfate, chloride, calcium, magnesium, potassium, sodium, silica, nitrate, nitrite, and phosphate. Chloride (Cl<sup>-</sup>) was analyzed on an unacidified aliquot of each sample. Magnesium (Mg<sup>2+</sup>) and calcium (Ca<sup>2+</sup>) were analyzed on both unacidified and acidified aliquots of the samples. All other shipboard analyses were performed on acidified aliquots. All dissolved constituents are expressed in units of millimoles per liter (mM) or micromoles per liter ( $\mu$ M). Table 5 contains a summary of analytical techniques used.

Alkalinity and pH were estimated using the Metrohm autotitrator with a Brinkman combination pH electrode. The slope of the electrode was calibrated and determined to be -58.95. Alkalinity and pH were determined immediately and in duplicate. In all cases the pH of borehole-fluid samples decreased from between 0.15 to 0.65 pH units between replicates. This was presumably due to the production of hydrogen ion during formation of iron oxyhydroxide precipitates and/or degassing of CO<sub>2</sub> from the samples. A similar decrease in alkalinity was observed between replicates and may be accounted for

**Table 5. Summary of analytical methods used for borehole fluid samples collected from Hole 504B during Leg 148.**

Analyte	Method	Precision 2σ
Cl <sup>-</sup>	AgNO <sub>3</sub> titration	7 mM
Mg <sup>2+</sup>	EDTA titration	1 mM
Ca <sup>2+</sup>	EGTA titration	0.1 mM
Alkalinity/pH	Metrohm auto titrator	0.1 mM
Salinity	Goldberg refractometer	
H <sub>2</sub> S	Precipitation as CdS, Cd by AAS	10 μM
NH <sub>4</sub> <sup>+</sup>	Colorimetric	5 μM
H <sub>4</sub> SiO <sub>4</sub>	Colorimetric	7 μM
PO <sub>4</sub> <sup>3-</sup>	Colorimetric	1 μM
NO <sub>3</sub> <sup>-</sup>	Colorimetric	2 μM
NO <sub>2</sub> <sup>-</sup>	Colorimetric	0.1 μM
Na <sup>+</sup>	Ion chromatography	8 mM
K <sup>+</sup>	Ion chromatography	0.5 mM
SO <sub>4</sub> <sup>2-</sup>	Ion chromatography	0.5 mM
CO <sub>2</sub>	Coulometer	0.05 mM
Fe	AAS	10 μM

by removal of hydroxide ion by iron-hydroxide precipitation. In all cases reported data are for the first measurement of pH and alkalinity. Precision is generally within 2%–3%.

Salinity was estimated using a Goldberg optical hand refractometer measuring the total dissolved solids. Chloride was measured by silver-nitrate titration of 1 mL of sample diluted with 5 mL of deionized water, using potassium chromate as an indicator. All titrations were carried out in duplicate or triplicate. Precision was better than 1%.

Sulfate (SO<sub>4</sub><sup>2-</sup>) was quantified using a Dionex-DX100 ion chromatograph. Precision on separate dilutions was better than 2%.

Calcium was determined by complexometric titration of a 0.5 mL sample with EGTA (ethylene-bis-[oxyethylenenitrilo]-tetra-acetic acid), using GHA (2-2'-ethane-diylindine-dinitrilo-diphenol) as an indicator. The calcium-GHA complex is extracted into a layer of butanol to facilitate detection of the endpoint. The corrections for strontium were carried out as described in Gieskes and Peretsman (1986). All samples were run in duplicate. Precision was estimated to be better than 1%.

Magnesium was determined by EDTA (di-sodium ethylenediamine-tetraacetate) titration for total alkaline earths. Subsequent corrections (Gieskes and Peretsman, 1986) for calcium and strontium yielded the magnesium concentration. All samples were run in duplicate. Precision was estimated to be better than 2% on replicates.

Hydrogen sulfide (H<sub>2</sub>S) was estimated by first precipitating the H<sub>2</sub>S from 15 g of sample as CdS with 100 μL of 1 M CdNO<sub>3</sub> solution to preserve the sulfide. The precipitate was washed and dissolved, and the resulting solution was analyzed for Cd by atomic absorption. Standards were made from Na<sub>2</sub>S and treated in the same manner as the samples and compared to solution standards of Cd with excellent results. The procedure allows determination of hydrogen sulfide to a concentration of 10 micromoles per liter (μM), with precision of 5% on replicates of the standard solutions.

Ammonium (NH<sub>4</sub><sup>+</sup>), silica (H<sub>4</sub>SiO<sub>4</sub>), nitrate + nitrite (NO<sub>3</sub> + NO<sub>2</sub><sup>-</sup>), nitrite (NO<sub>2</sub><sup>-</sup>), and phosphate (PO<sub>4</sub><sup>3-</sup>) were determined by the spectrophotometric techniques described in Gieskes and Peretsman (1986). Sodium and potassium were determined by flame atomic emission spectrometry. Standards were made from dilutions of standard seawater. Standard seawater was run every two samples to adjust for instrumental drift using the provided software. Samples and standards were diluted to 10,000 × with 0.5% cesium chloride added as an ionization buffer. Precision was estimated to be ±5% for potassium and ±2% sodium.

Magnesium, calcium, potassium, and sodium were also run on the Dionex DX-100 ion chromatograph. This instrument was brought on board for Leg 148 to replace the Dionex 2120, primarily for the anal-

ysis of sulfate. Cation analysis was run for comparison to classic techniques during method development of this new instrument. All samples were run on 1:200 dilutions. All samples and standards were run in duplicate. Standards were run as samples at the start and end of each run to test for drift. No significant drift was noted; final standard concentrations were within expected values. Excellent agreement was obtained for both Ca and Mg compared with titration results. However, the results of the titrations are reported to maintain consistency with past results. Sodium and potassium results have much greater precision using the DX-100 than by atomic absorption methods yielding inter-run precision of 0.5% for sodium and 1.25% for potassium. For this reason the results of the ion-chromatograph are reported for sodium and potassium data.

Dissolved carbon dioxide in the fluid samples was analyzed using the Coulometrics CO<sub>2</sub> Coulometer, following the procedure outlined in the instrument manual. Standards were made from dried analytical-grade sodium bicarbonate. Samples were taken in zero-head-space-glass vials fitted with clamp-on septum caps. A gas-tight glass syringe injected 5 mL of sample/standard into the septum fitting on the coulometer extraction apparatus. Carbon dioxide was driven out of the sample by adding 5 mL of 2N HCl. During calibration nanopure water blanks were run, yielding values of 4–8 μg C after allowing the coulometer to run for 15 min. Standardization of the 216 μg C/mL yielded a concentration of 214 μg C/mL, showing the excellent accuracy of this method. Replicates of samples and standards yield a precision of 5% based on 2 × the standard deviation of replicates.

## IGNEOUS AND METAMORPHIC GEOCHEMISTRY

### X-ray Fluorescence Analyses

The shipboard party selected samples that were considered to be representative of the individual lithological units or of unusual composition; the samples were subsequently analyzed by X-ray fluorescence spectrometry (XRF) for major and selected trace elements. All of the samples collected during Leg 148 were analyzed using the Philips PW1400 fully automated wavelength X-ray spectrometer in

**Table 6. XRF spectrometer conditions employed at Nottingham University.**

Element	Line	kV	mA	Crystal	Col.	Det.	Pk.	Bkg.
Fusion Bead								
Si	K(a)	40	70	PE	C	F	20	4
Al	K(a)	40	70	PE	C	F	16	2
Ti	K(a)	40	70	LiF200	F	F	20	10
Fe	K(a)	60	50	LiF200	F	F	16	6
Mg	K(a)	40	70	TIAP	C	F	40	16
Ca	K(a)	40	70	LiF200	C	F	10	2
Na	K(a)	40	70	TIAP	C	F	40	10
K	K(a)	40	70	PE	C	F	10	2
Mn	K(a)	60	50	LiF200	C	FS	10	8
P	K(a)	40	70	GE	C	F	10	4
Pressed Pellets								
S	K(a)	40	70	PE	C	F	20	10
Sc	K(a)	55	35	LiF220	F	F	80	40
V	K(a)	40	70	LiF200	F	F	40	20
Cr	K(a)	50	60	LiF200	F	F	40	20*
Ni	K(a)	70	40	LiF200	C	FS	20	8
Cu	K(a)	70	40	LiF200	F	FS	20	10
Zn	K(a)	75	40	LiF220	F	S	40	20
Ga	K(a)	75	40	LiF200	F	FS	40	20
Rb	K(a)	75	40	LiF200	F	S	40	20*
Sr	K(a)	75	40	LiF220	F	S	40	20*
Y	K(a)	75	40	LiF220	F	S	40	20*
Zr	K(a)	75	40	LiF220	F	S	40	20
Nb	K(a)	75	40	LiF220	F	S	40	20*
Ba	L(b)	50	60	LiF220	C	F	40	20

Notes: Line: (a) = alpha line, (b) = beta line; Col. = Collimator, C = coarse, F = fine; Det. = Detector, F = gas-flow proportional counter, S = scintillation counter; Pk. = peak counting time; Bkg. = background counting time, both of which are in seconds; \* indicates that the background is sloping, such that the background was measured on both sides of the peak; X-Ray tube: side window 3kW Rhodium.

the Department of Mineral Resources Engineering, University of Nottingham, U.K. This situation arose due to severe stability problems with the shipboard XRF. The operating conditions that are used for routine XRF silicate analyses at Nottingham University are listed in Table 6. The major element analyses were performed on glass fusion beads and trace elements on pressed powder pellets.

### Crushing and Grinding

Following cutting of samples by either water-cooled saws or 1-in.-diameter diamond drill cores, samples were wet-ground on diamond abrasive wheels to remove saw marks and any unwanted material. The average sample taken weighed approximately 22 g. After grinding, the samples were sonicated in distilled water and methanol for 10 min each, followed by drying at 110°C for at least 2 hr. Larger pieces were reduced to <1-cm diameter by crushing samples between two discs of Delrin plastic in hydraulic press. Powders were produced by grinding samples for approximately 2 min in a tungsten carbide shatterbox. Sample contamination from the tungsten carbide shatterbox is only significant for W, Co, and Ta (Thompson and Bankston, 1970); the grinding times appear to be too short to produce significant Nb contamination (<1 ppm).

### Major elements

The major elements were determined on glass fusion beads following the procedure of Harvey et al. (1973); this approach was used in order to reduce matrix effects and eliminate particle size effects (Norrish and Chappell, 1976). The rock powders were dried at 110°C for 12 hr prior to analysis, then 0.37 g of material were weighed into Pt-Au crucibles and placed in a furnace at 1050°C for 1 hr. The samples were then removed and allowed to cool in sealed desiccators, the samples were then re-weighed to determine the loss on ignition (LOI); 2.1 g of dried (6 hr at 400°C) spectroflux 105 were added. Spectroflux 105 is composed of 47% lithium tetraborate, 36.7% lithium carbonate, and 16.3% lanthanum oxide, has a melting temperature of 715°C, and acts as a heavy absorber. The cocktail of sample and flux was then returned to the furnace (1050°C) for 45 min. Individual crucibles were then removed and placed on a blast burner in order to thoroughly mix the molten material and to remove air bubbles. Following labeling, the samples were presented to the XRF for analysis. In this procedure the LOI value is an integral part of the analysis. The LOI value in part reflects the volatile content of the

sample (i.e., H<sub>2</sub>O and CO<sub>2</sub> content), but it is also influenced by the oxidation state of elements such as Fe and S. In some analyses it is possible to obtain negative LOI values, which in the case of the present sample probably indicates that the majority of the Fe present was in the +2 state.

In the laboratory, sets of international standards are prepared in the same manner for each batch of flux.

### Trace Elements

Trace elements were determined on pressed-powder pellets using the method of Brewer (1985). The pressed pellets were made by mixing 8- to 10-g pellets of homogenized rock powder with a few drops of an inert PVP-methyl cellulose binder. This mixture was then pressed between two 31.5 mm stainless steel platens in a hydraulic press to 10 tons. The pellets were then dried for 30 min in an oven at 110°C. By using 8- to 10-g pellets, "infinite" thickness can be achieved for XRF analysis. A range of international standards have also been prepared using the same procedure.

Both the major and trace elements were analyzed using a 3 KW Rh X-ray tube and using an absorption correction based on Compton ratios (Harvey and Atkin, 1983). In order to estimate the precision and accuracy of the technique a set of international standards were run with both the major and trace elements (Table 7).

### Preparation of Inter-laboratory Geochemical Standard

To facilitate future comparisons between geochemical data generated at the many different laboratories participating in research related to Leg 148, an inter-laboratory geochemical standard was prepared from approximately 1 kg of diabase (Sample 137-504B-182M-3, 7–20 cm), following the procedures outlined above. After grinding, accumulated batches of rock powder were homogenized in a 1-gal sealed plastic freezer bag for about 1 hr and then distributed in roughly 30 g aliquots to interested members of the shipboard party. Analytical results from the participating labs will be reported in the Leg 148 *Scientific Results* volume.

### Carbon and Water Analyses

Total carbon, as CO<sub>2</sub>, and structural water (H<sub>2</sub>O<sup>+</sup>), were determined using a Carlo Erba NA 1500 CHNS analyzer. Nitrogen and sulfur concentrations in the investigated rocks were usually below the

**Table 7. Summary of some of the international standard values obtained during the analysis of Leg 148 samples.**

	PCC-1	BHVO-1	GSP-1	MRG-1	NIM-G	Detection Limit
SiO <sub>2</sub> (wt%)	42.01	49.91	67.75	39.06	75.71	0.01
Al <sub>2</sub> O <sub>3</sub>	0.74	13.77	15.33	8.46	12.06	0.01
TiO <sub>2</sub>	0.01	2.73	0.67	3.75	0.10	0.01
Fe <sub>2</sub> O <sub>3</sub>	8.60	12.23	4.34	17.91	2.01	0.01
MgO	44.22	7.25	1.02	13.57	0.02	0.01
CaO	0.62	11.38	1.93	14.93	0.78	0.01
Na <sub>2</sub> O	0.01	2.25	2.85	0.72	3.39	0.01
K <sub>2</sub> O	0.01	0.53	5.57	0.18	5.00	0.01
MnO	0.12	0.17	0.03	0.16	0.02	0.01
P <sub>2</sub> O <sub>5</sub>	<0.1	0.28	0.28	0.07	0.01	0.01
Sc (ppm)	10	29	5	55	1	1
V	29	315	53	526	<2	3
Cr	2750	290	13	430	11	3
Ni	2400	121	10	193	9	2
Cu	11	135	32	135	13	1
Zn	44	104	102	191	50	3
Ga	2	20	23	17	27	1
Rb	1	10	246	9	318	1
Sr	<1	396	234	266	101	1
Y	<1	28	27	13	144	1
Zr	9	176	527	109	297	3
Nb	1	18	28	21	53	1
Ba	<8	137	1252	58	117	8

**Table 8. Calculated detection limits and estimates of precision for the Leg 148 H<sub>2</sub>O<sup>+</sup>, and CO<sub>2</sub> analyses.**

Wt%	Estuarine sediment			Diabase BAS 140		
	Mean	1σ	Relative standard deviation	Mean	1σ	Relative standard deviation
H <sub>2</sub> O	6.12	0.37	6.1	1.41	0.016	1.1
CO <sub>2</sub>	6.37	0.28	4.4	0.072	0.011	15.6

detection limit of the CHNS analyzer. Fifty to 80 mg of dried (110°C) bulk rock samples were combusted at 1010°C under an oxygen atmosphere, converting organic and inorganic carbon into CO<sub>2</sub> and thermally releasing H<sub>2</sub>O. Following gas-chromatographic separation of the gases, CO<sub>2</sub> and H<sub>2</sub>O<sup>+</sup> were quantitatively determined using a thermal conductivity detector. The bias factor (K) of the CHNS-analyzer was calculated by measuring CCRMP reference gabbro, MRG-1 (CO<sub>2</sub> = 1 wt%; H<sub>2</sub>O<sup>+</sup> = 0.98 wt%).

Analyzed samples were typically splits taken from powders prepared for XRF analysis. Two replicate measurements were performed on each sample. Accuracy was checked with reference rocks (Table 8). Reproducibility was tested by analyzing the shipboard basalt Sample AII92 29-1 (Staudigel, 1979). The relative standard deviation of 17 replicate analyses was about 9% for both CO<sub>2</sub> and H<sub>2</sub>O<sup>+</sup>.

**STRUCTURE AND DEFORMATION**

**Introduction**

The structural geology of the core recovered from Hole 504B on Leg 148 is crucial to our understanding of oceanic spreading centers and of the igneous and metamorphic processes active in the genesis of the lower crustal sequence in particular. Specialist structural studies are not standard procedure on ODP legs. An exception is Leg 131 (Nankai Trough), where specific objectives that could potentially be addressed by structural studies were identified from the outset. However, in general, standardization of methodology or nomenclature for the structural geological description of ODP core is absent. For Leg 148 we adopted a convention for the measurement and description of core that is a modification of the procedures developed on Legs 140 and 147.

This section outlines the techniques used for macroscopic and microscopic description of structures, the conventions adopted for measurement of planar and linear structural features, and the methods used to reorient core to its original geographical coordinates.

**Nomenclature**

In an attempt to achieve consistency in nomenclature, we adopted the following working terminology for macroscopic structures in the initial core description:

**Table 9. Deformation categories used in macroscopic core description.**

Category	0	1	2	3
Magmatic Crystal-Plastic Cataclastic	Isotropic; no shape fabric Crystallographic fabric absent Undeformed	Weak shape fabric Weakly foliated Crush breccia; dense anastomosing fracturing and incipient breccia; minor translation possible	Moderate shape fabric Strongly foliated (protomylonite) Microbreccia; well-developed fault brecciation; rotation of clasts necessary	Strong shape fabric Porphyroclastic mylonite Protocataclastic: rotation, translation and grain-size reduction
Fractures Density Displacement	No fractures Unfractured	Occasional fractures Minor fracturing no observable displacement	Moderate fracturing Minor observable displacement (fault)	Abundant fracturing Major faulting
Veins Density Displacement	No veins No displacement	Occasional veins (= filled fractures) No displacement, minerals bent	Moderate veining Displacement, no growth fibers (slickenfibers)	Abundant vein networks Displacement, undeformed growth fibers

1. Igneous contacts
2. Cataclastic features
3. Veins
  - A. Vein density
  - B. Displacement
4. Fractures (no vein material)
  - A. Fracture density
  - B. Displacement

This nomenclature for rock fabrics (shown in Table 9) is modified from the nomenclature used for Legs 140 and 147, which in turn was extensively modified from that established for gabbros from Leg 118 (Dick et al., 1991). We have subdivided the fracture and vein category into displacement and density subcategories. The vein density subcategory is equivalent to the vein category of Legs 140 and 147. We added the displacement sub-category because some veins in samples from Hole 504B show offset without any cataclasis, and in some cases they contain parallel mineral fibers (growth fibers or slickenfibers). We distinguish brittle deformation by cataclasis (i.e., grain-size reduction due to frictional sliding) and simple fracturing along discrete surfaces (with or without minor shear). We restrict the term fracture to open planar features without any mineral fill. Fault rocks are classified using the criteria of Sibson (1977; Fig. 8): (1) whether they are incohesive or cohesive; (2) the proportion of matrix; and (3) whether or not the rock is foliated. Figure 8 illustrates the change with increasing pressure and temperature from the breccia-gouge series to

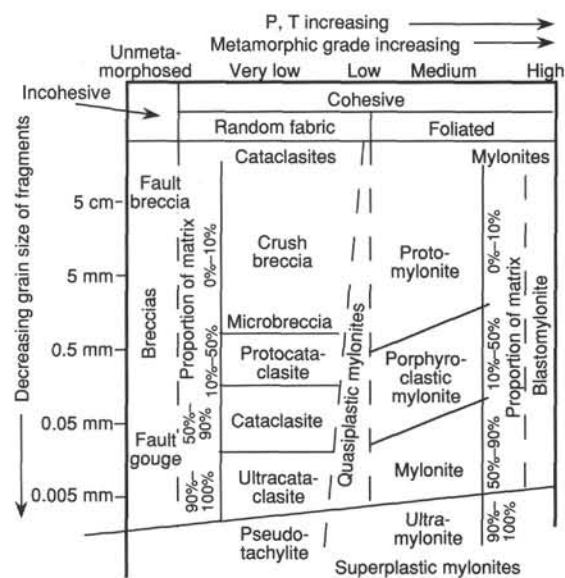


Figure 8. Fault-rock terminology, modified from Sibson (1977).

the cataclastic, and finally to the mylonitic series. We do not include the breccia-gouge series in the deformation log because incohesive fault rocks are unlikely to be recovered during drilling. Note that vein-faults represent a separate class of faults which are not represented in Figure 8. Vein-faults may form by filling of a pre-existing shear fracture, but they can also form from repeated cycles of hydraulic fracturing (crack-seal mechanism), resulting in growth fibers (slickenfibers) oriented parallel to the slip direction (Cox and Etheridge, 1983). True extension veins can also form by this mechanism, in which case the fibers are oriented normal to the vein wall. Recognition of veins formed by the crack-seal mechanism is important for the following reasons: (1) they imply high pore pressures and hydraulic fracturing; and (2) they can form at much lower shear stresses than those required for frictional sliding (Cox and Etheridge, 1983).

In many respects the deformation processes in mylonitic and cataclastic shear zones are similar, with the exception that crystal-plastic deformation and dynamic recrystallization do not take place in the latter. Accordingly, we have erected a parallel classification scheme for cataclastic and crystal-plastic textures (Table 9).

Veins are characterized according to their fill, their width, the presence or absence of an alteration halo, whether there is any offset across the vein, and whether they contain growth fibers. Fractures may represent natural joints, drilling-induced fractures, or discrete faults with minor offset: the latter are distinguished on the basis of reasonable evidence for displacement, including truncation or offset of markers and presence of slickenlines (care was necessary to distinguish the latter from drilling-induced polishing striations).

By subdividing structures in this manner, we are not implying that these features fall into distinct and exclusive categories. Clearly there is gradation and even overlap, but particular aspects are emphasized by adding modifiers, descriptive comments, and sketches.

### Macroscopic Core Description

Structural records identify and describe in a systematic and quantitative way all structural information present in the core, and in particular record the orientation of structures relative to the core axis and, where possible, geographic coordinates (using paleomagnetic measurements). All material from both working and archive halves was examined, although most measurements were made on the working half. Initial data were recorded on a working structural log and a deformation log. The logs are included as appendixes to the site chapters. Data recorded on these logs were later entered into separate spreadsheets. The logs were updated during the course of the leg as more data became available. Detailed observations and sketches are recorded on separate sheets as shown. The most pertinent observations are included in the text, and copies of the original hand specimen descriptions can be obtained from the ODP database. In addition, each particular type of structural observation was made by the same individual to ensure consistency of observation throughout the recovered section.

The following sections explain the structure and deformation logs, and provide a summary of the procedures used as well as insights into

the difficulties and constraints encountered when dealing with structures observed only in core.

### Structural Core Description Log

The structural core description log is essentially the same as the log used on Leg 140. A definition of the various columns in the structural core description form is given in Table 10. The location of an individual structure was recorded in centimeters from the top of the section, according to ODP procedure. Where a structure extended over an interval, the locations of the top and bottom of its range on the cut face of the core were recorded. The sense of fault displacement was also recorded where the direction of motion (from mylonite lineations or slickensides) could be determined.

Several problems are inherent in any study of this nature. From the point of view of identification of tectonic features, commonly only part of the sampled interval in any one core is actually recovered, which leads to a sampling bias that for structural purposes is particularly acute: material from fault zones may be missing when recovery is less than 100%. When faulted or fractured rock from such zones is recovered, its orientation is commonly highly disturbed relative to its original position.

Determining the orientation of observed structures is also problematic. Features must initially be oriented relative to local reference coordinates (i.e., the core barrel reference frame) and subsequently corrected to true north and true vertical. The drilling process causes fracturing and rotation of core such that relative rotations in any individual section or core barrel have occurred and corrections back to true north may be different for each piece of a core. Furthermore, the reference line for each piece is drawn arbitrarily, following visual inspection by the structural geologists, so this temporary reference orientation may potentially be consistent over only a few tens of centimeters.

### Measurement of Structures

Measurement of planar features traversing the core at oblique angles can be made in several ways. The convention used on Leg 148 (Fig. 9) is adapted from that used during Legs 131 and 134, and subsequently modified during Legs 135 and 140. We used a simplified version of the protractor-based instrument described in the Leg 131 *Initial Reports*. The plane normal to the axis of the borehole is referred to as the apparent horizontal plane. On this plane a 360° net is used with a pseudo-north (000°) at the bottom line of the working half of the core, the same practice as is used for shipboard paleomagnetic studies. The face of the split core, therefore, lies in a plane striking

Table 9 (continued).

Category	4	5
Magmatic		
Crystal-Plastic	Mylonite	Ultramylonite
Cataclastic	Cataclasis	Ultracataclasis
Fractures		
Density		
Displacement		
Veins		
Density		
Displacement	Displacement, growth fibers deformed	

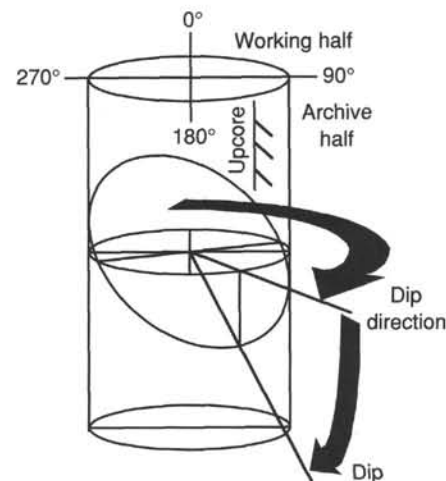


Figure 9. Convention used for the measurement of azimuths and dips on structural features in basement core.

**Table 10. Definitions of working core-description fields.**

1.	Core number and type.
2.	Section number.
3.	Piece number. A symbol of an "x" in a circle is used if the piece is not oriented with respect to the vertical. A feature occurring on more than one piece is recorded as the piece on which it was measured, and the range of pieces on which it occurs is noted in the comments field.
4, 5.	Interval in centimeters that the feature covers on the cut face. Where the interval is less than 1 cm, only the depth to top of the feature is recorded.
6.	Feature type (e.g., vein, fracture, fault) and composition of material within structure (e.g., fault gouge, vein fill). Abbreviations used are those defined in the "Igneous and Metamorphic Petrology" section, this chapter.
7.	Orientation of feature. Normally two apparent dips are measured and recorded in a dip direction/dip angle convention. The true dip is then calculated using a stereonet computer program and recorded in brackets on the sheet as dip direction/dip angle. If it is possible to measure the true dip directly, it is recorded in the brackets without apparent dips. If the vertical axis on a non-oriented piece can be determined, apparent dips are recorded and true dip calculated as with the oriented pieces, but only the dip angle is recorded and a dash entered in place of the dip direction.
8.	Shear/Method: Sense of movement and indicator (e.g., slickensides or rotated porphyroclasts) for faults and mylonite zones.
9.	Comments and sketches. Comments regarding the continuity and the form of the feature are usually recorded, as well as pertinent information on thickness, offsets, and crosscutting relationships. Fractures of the "tiny white crack" variety are noted by the initials TWC. If necessary, a sketch of the piece identifying the features is drawn. It is also noted by the initials HSD (hand specimen description) if a more detailed drawing and description of that piece has been done.

090°–270° and dipping vertically. An apparent dip can be measured on this surface and its sense (toward 090° or 270°) indicated. Unless the fracture, vein, etc., strikes 000° so that true dip can be measured directly on the face of the split core, measurement of one further apparent dip on whatever surfaces are accessible is required to obtain a (relative) orientation, as described above. Where a structure was evident as a three-dimensional plane in a fragmented piece of core, or its trace could be observed at the top or bottom of a core section, the strike and a single apparent dip were measured. Direct strike measurements are preferred wherever possible because they are much more precise; the derivation of a plane by the combination of two apparent dips is subject to uncertainty in the dip direction if the dip of the plane is shallow. When required, a thin (~1 mm thick) sliver was shaved from the edge of oriented pieces of the working half of the core, orthogonal to the cut surface, providing a second surface from which apparent dips could be accurately determined. Dips recorded at this stage assume that the core was vertical; if other data (e.g., data generated by the general purpose inclination tool, GPIT) suggest otherwise at a later stage, a correction can be made on the spreadsheet template. True dips were derived stereographically, using the Stereonet Plotting Program of R.W. Allmendinger, Version 4.1-11. The two apparent-dip orientations were entered as lines, and the computer generated the great circle defined by the lines. The orientation of this great circle gave the true dip of the observed structure and the working dip direction, both of which were recorded on the structural log and entered into the spreadsheet. In some small pieces the vertical axes could be identified from their cylindrical shape, but not the up direction, as they may have rolled in the core barrel (this was a particular problem during this leg, because no core liner was used). In these pieces the true dip of planar features was recorded, but not the direction of dip.

Mineral foliations and lineations can be measured in much the same way as faults and veins. True orientations can generally be measured directly because the core is generally chosen to be split parallel to lineations or perpendicular to foliations, though none were encountered on this leg.

Linear structures such as slickensides can be measured in a similar fashion: either directly, by their azimuth and amount of plunge, or indirectly, by means of their pitch on a previously measured plane. The sense of movement can often be ascertained from slickensides using the criteria of Petit (1987). The magnitude of displacement may be

measured directly if the fault surface is visible, or it can be calculated from the apparent displacement on the cut surface of the core.

#### *Orientation of Core*

Correction of the "working dip direction" (i.e., the trend of a line parallel to the direction of dip) to real geographical coordinates may be accomplished by use of both paleomagnetic and downhole logging data. We have used the stable, high-coercivity components of the magnetization measured from discrete minicores (see "Paleomagnetism" section, this chapter) as an external reference frame, but we are well aware of the problems associated with such a procedure. The crust sampled at Hole 504B was formed at an oceanic spreading axis close to the equator. The upper crustal sequence carries a reversed magnetization; thus the expected reference direction for the remanence is approximately horizontal and to the south. The same may not be true for the lower crustal rocks, which may carry a normal remanence: this would introduce an error of 180° to the core orientation.

Another problem involves the effect of a tilt on a paleomagnetic direction. In most situations a simple tilt about a horizontal axis will affect the declination as well as the inclination. We are fortunate that the crust at Hole 504B formed at an east-west spreading center: any tilting is likely to have been towards the north or south, thus causing only a minor shift in declination of a south-trending magnetic vector.

Within the plutonic sequence, rocks that carry a significant fabric can show deviation of the magnetic remanence away from the applied field due either to the influence of a previously existing magnetic fabric on the acquisition of the remanence or to a subsequent rotation effect. These processes are poorly understood and difficult to correct. For this reason we suggest that, wherever possible, relatively isotropic rocks should be sampled.

The logging program on Leg 148 included the Formation MicroScanner (FMS), a tool that makes an image of the borehole wall by measuring variations in resistivity by means of pads pressed against the wall (see "Downhole Measurements" section, this chapter). The FMS carries fluxgate magnetometers that allow orientation of the processed images. The FMS can be used in its own right as a structural tool, and it is also of use in orienting sections of core. The difference between the diameter of the borehole and that of the core is such that identification of individual features on both cannot be made directly and may be difficult. The FMS tool can be used most

successfully for orientation purposes when, for example, a single, regular joint or layering pattern can be recognized on downhole images and correlated with core-derived data.

Downhole logging is most powerful in this context when used in conjunction with paleomagnetism, because it potentially allows identification of possible tectonic rotations of the magnetization vector, which otherwise would have to be assumed to be zero. The hard-rock orientation tool brought on Leg 148 is still in its development stage and was unsuccessful in the one hole on which it was used (Hole 896A).

### Deformation Log

The deformation log was designed to provide a continuous record of the style and intensity of deformation. The Leg 148 deformation log is based on the deformation log used during Leg 140, but it was modified to include the deformation types and categories used on Leg 147 (Table 9). The Leg 147 and 148 Shipboard Parties distinguish between fabrics defined by the preferred orientation of the long axes of inequid crystals formed in response to magmatic flow, and crystal lattice fabrics formed by solid-state deformation processes; other individuals (e.g., Robinson, Von Herzen, et al., 1989) did not make this distinction. We established separate categories to reflect these different mechanisms of fabric development (Table 9). Only isotropic crystallographic fabrics were encountered on this leg.

We delineated three types of brittle structures: cataclasites, fractures, and veins, which have been discussed above (see "Nomenclature," this section). Cataclasites are further subdivided into the following, based on the proportion of matrix: crush breccia, microbreccia, protocataclite, cataclite, and ultracataclite (Table 9 and Fig. 8).

### Thin-Section Descriptions

Thin-section billets of basement lithologies recovered during Leg 148 were examined for the following: (1) to confirm macroscopic descriptions of ductile and brittle structures; (2) to provide basic information on the kinematics of brittle and/or ductile deformation; (3) to identify relative age relationships between magmatic, deformation (brittle and ductile), and alteration processes; and (4) to provide coverage of major structural zones and a representative section of downhole variations. Where possible, sections were oriented with respect to the core (i.e., the original vertical is preserved). A standard form was used to ensure consistent description of microscopic features based on the fields described in Table 9. Comments and sketches are included wherever appropriate, similar to the procedure used on Leg 140 (Dick, Erzinger, Stokking, et al., 1992).

The thin-section observations are summarized in the site chapters (this volume), and observations are included in the text. Copies of the original thin-section descriptions can be obtained from the ODP database.

## PALEOMAGNETISM

Paleomagnetic measurements were performed on vertically oriented minicore samples and unoriented pieces that were chosen to be representative of the lithology and alteration mineralogy of Leg 148 cores. Additionally, an effort was made to select samples near important structural features so they could be oriented using paleomagnetic directions. At least one minicore sample (diameter 2.5 cm, length 2.2 cm) or unoriented piece was taken from each section of core for shipboard study. For many of the hard-rock cores, the only true orientation is with respect to the vertical dimension. This is because individual pieces of the core are free to rotate within the core barrel and thus are not oriented with respect to north, or to each other. In some sections (see "Operations" section, this chapter), the hard-rock orientation (HRO) system was used to orient the core. This provided an external reference frame to which the observed magnetic directions

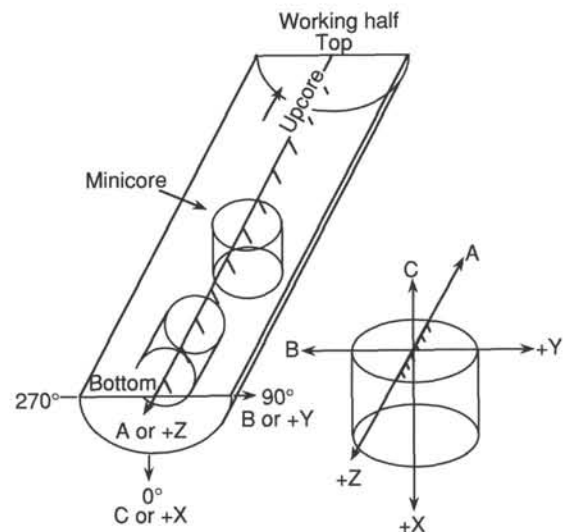


Figure 10. Orientation diagram and terminology used for paleomagnetic and physical properties measurements.

could be corrected. After splitting individual pieces of the core, ODP convention for rotary cores follows that of an oriented piston core (see Fig. 10). That is, +X (north) is directed into the face of the working half of the core, +Y (east) points toward the right side of the face of the working half of the core, and +Z is down. A full suite of magnetic measurements (see below) were conducted on the oriented minicores, whereas measurements on unoriented pieces were limited to bulk susceptibility and intensity of natural remanent magnetism (NRM).

### Measurement of Remanent Magnetization

Two magnetometers, a Molspin spinner magnetometer and a 2-G Enterprises (Model 760R) pass-through cryogenic rock magnetometer, were used to measure remanent magnetization of the samples. The superconducting quantum interference device (SQUID) sensors in the cryogenic magnetometer measure the intensity and direction of magnetization over an interval approximately 20-cm long. During Leg 148, the SQUID electronics were operated in the flux-counting mode. An alternating field (AF) demagnetizer (Model 2G600) capable of producing an alternating field up to 20 mT can be used on-line with the pass-through cryogenic magnetometer. The magnetometer, the demagnetizer, and their common stepper motor transport system were operated over serial interfaces by software on an IBM-compatible personal computer. The software was an ODP customization of a QuickBasic program provided by 2G, originally called SUPERMAG. The first batch of three samples was demagnetized up to 20 mT using the Model 2G600 AF demagnetizer, but as these acquired a spurious anhyseretic remanent magnetization (ARM) component, all further AF cleaning was done using a single-axis Schonstedt Geophysical Specimen Demagnetizer (Model GSD-1) at 2.0, 5.0, 10.0, 15.0, 20.0, 25.0, and 30.0 mT, and upward in 10 mT increments, to a maximum attainable field of 100 mT. Results were analyzed using the program Magraph (provided by H. Shibuya, Leg 124), which allowed stable components to be calculated using linear regression. Initial NRM intensities were corrected for a correct volume calculated by Archimedes's Principle (see "Physical Properties" section, this chapter).

### Measurement of Bulk Magnetic Susceptibility and Anisotropy of Magnetic Susceptibility

The volume magnetic susceptibility ( $K$ ) and the susceptibility tensor ( $K_{ij}$ ) were measured on standard-sized minicores (2.4 × 2.2 cm) using a Kappabridge KLY-2 (Geofyzika Brno). The Kappabridge is a

semi-automatic autobalance inductivity bridge with a high sensitivity ( $4 \times 10^{-8}$  SI units) and an accuracy of  $\pm 0.1\%$  within one measuring range. The induced magnetization of the specimens is determined in 15 positions in a field of 300 A/m and the susceptibility tensor ( $K_{ij}$ ) is calculated from the measurements. The principal magnitudes and directions of  $K_{ij}$  were obtained by the diagonalization of the tensor; the principal directions are given by the eigenvectors and the principal magnitudes by the eigenvalues. The bridge is interfaced with an IBM-compatible personal computer. Data is collected and processed using the FORTRAN-77 program ANI20 written by V. Jelinek. To avoid problems associated with the impression of a magnetic susceptibility anisotropy by alternating fields (i.e., Potter and Stephenson, 1990) the AMS measurement was completed before any other magnetic measurements, particularly static AF demagnetization, were conducted. Volume susceptibilities were corrected for true volumes calculated from Archimedes's Principle.

The low-field susceptibility values were used in conjunction with the values of the intensity of NRM ( $J_0$ ) to calculate the Koenigsberger ratio,  $Q$ , of the samples. A field value of 0.032 mT was assumed for Site 504 so that  $Q = J_0 \times 4\pi / (\times 0.032 \times 10^4)$ .

### Rock Magnetic Measurements

The relatively low recovery rate on Leg 148 gave us time to complete a series of rock magnetic measurements that are not standard procedure on ODP legs. We completed measurements of ARM, demagnetization of ARM, and isothermal remanent magnetization (IRM) on the minicores from the Leg 148 cores. Most of this additional work was done after the physical property measurements of density, sonic velocity, and electrical conductivity had been completed, but before the samples were heated to about 110°C. The ARM measurements were made using the Schonstedt AF demagnetizer and a DTECH double-coil device, which allowed a steady, unidirectional field of 0.032 mT to be applied during each AF step. The ARM was acquired during progressive steps of increasing AF field, up to 90 mT, and the magnetization was measured in the cryogenic magnetometer between each step. Demagnetization of ARM was conducted in a similar fashion.

The IRM acquisition experiments were accomplished using the ASC impulse magnetometer (Model IM-10). Samples were subjected to a steady magnetic field along the +X axis and measured using the Molspin spinner magnetometer. This process was repeated for progressively increasing fields, up to 1.2 T.

### PHYSICAL PROPERTIES

Compressional-wave ( $P$ -wave) velocities, index properties (bulk density, porosity, water content, and grain density), thermal conductivities, and resistivities were measured for the crystalline rocks recovered during Leg 148. Experimental details are described below and in the cited references.

#### Compressional-wave Velocity

The pulse transmission method was employed to determine the compressional-wave velocity using piezoelectric transducers as sources and detectors in a screw-press Hamilton Frame described by Boyce (1976). All measurements were made on water-saturated samples at zero confining pressure. Calibration measurements were performed using plexiglas and aluminum minicores to determine the zero displacement time delay inherent in the measuring system. The traveltimes through a range of different lengths of each material were measured (Table 11) and plotted on a time-distance graph (e.g., Fig. 11). An average of the intercept at zero length for both materials gives the delay time for the particular set of transducers. This technique has been used previously for measurements in Hole 504B (Shipboard Scientific Party, 1988a) and is preferable to taking a single reading at zero length. Early tests indicated that the flatness and parallelism of

**Table 11. Calibration measurements for the Hamilton Frame velocimeter.**

Calibration data		
Leucite	Length (mm)	Traveltime ( $\mu$ s)
	9.97	
	20.05	8.85
	30.04	12.55
	40.14	16.40
	50.07	20.20
	65.74	26.05
Least squares fit: Time = 1.246 + 0.378 length		
Aluminum	Length (mm)	Traveltime ( $\mu$ s)
	20.00	4.55
	40.00	7.75
	50.00	9.35
	60.00	10.90
Least squares fit: Time = 1.380 + 0.159 length		
Average delay: 1.313 $\mu$ s		

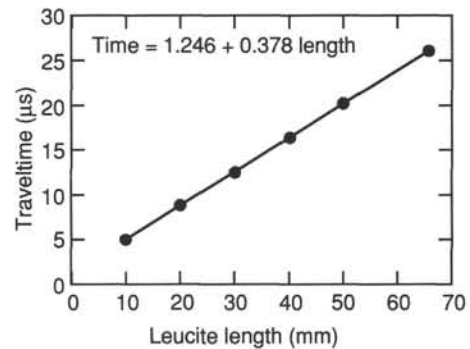


Figure 11. Calibration plot used for the Hamilton Frame velocimeter.

the specimens determined the accuracy and reproducibility of the measurements. Accordingly, the samples were prepared with both sides flat and parallel to within 0.08 mm. This small tolerance resulted in sharply defined first arrivals of the direct compressional-wave mode.

Shipboard compressional-wave velocity measurements are usually obtained in three orthogonal directions ( $A$ ,  $B$ , and  $C$  transmission directions) as shown in Figure 10. Because of sampling limitations, only one type of minicore (25.3-mm diameter and 15- to 40-mm long) was used during Leg 148: samples drilled normal to the core splitting plane (i.e., horizontal). Measurement uncertainties in transmission length ( $\pm 0.08$  mm,  $\pm 0.25\%$  of length) and timing uncertainties ( $\pm 0.035$   $\mu$ s or 0.1%) yielded nominal uncertainties in compressional-wave velocity ( $V_p$ ) of about 0.3%. Calibration against leucite standards ( $V_p = 2.745$  km/s) were reproduced to within 0.3%. Measurement of  $V_p$  in an aluminum standard resulted in a velocity of  $6.260 \pm 0.035$  km/s, about 0.5% lower than the nominal velocity of 6.295 km/s. In practice, heterogeneity of the rock samples and irregularities in the sample shapes and finishes degrade the experimental accuracy to about 0.8% or 0.05 km/s.

#### Index Properties

Dry- and wet-bulk densities were determined for all minicore samples using motion-compensated microbalance measurements of mass ( $\pm 0.002$  g accuracy) and sample volumes ( $\pm 0.03\%$ ) calculated from the weight loss in water. The porosity and water content of each minicore were then determined from the weight loss after drying at  $110^\circ\text{C} \pm 50^\circ\text{C}$  for 24 hr. Porosities were determined to no better than  $\pm 0.2\%$ , assuming that the porosity is interconnected and fluid-saturated. Grain densities were then calculated from the dry density and porosity of each sample. Salt corrections were not applied because they are insignificant at the low porosities encountered on Leg 148.

## Thermal Conductivity

Core samples were measured nondestructively for thermal conductivity in the shipboard laboratory. Specimens were obtained from the archive half in order to keep samples used for chemistry analyses from being contaminated with thermal conductive grease. This technique was previously used during Leg 129 and is documented in the shipboard thermal-conductivity manual. Measurements were performed over a 6 min period with a heated needle probe sandwiched between the sample and a slab of low-conductivity material (Vacquier, 1985). This method is most convenient for the hard-rock cores, which were cut in the form of a half-round cylinder because this shape is easily adapted to the apparatus. The flat surface was polished in order to provide good thermal coupling between the sample and the needle probe.

The theory of the method closely approximates the heating of a line source in a plane separating half-spaces of the sample material and a thermal insulator, which in turn is a relatively straightforward extension of the method of heating a uniform full-space by a line source (Jaeger, 1956; Von Herzen and Maxwell, 1959). If the substrate on which the sample is placed were a perfect thermal insulator, the rise in temperature with time at the needle probe would be exactly twice that measured by the probe in an infinite medium having the same thermal conductivity as the sample. The thermal conductivity is then estimated by calculating the slope of the best-fit straight line to a plot of temperature vs. the natural logarithm of time, where the value of the slope is inversely proportional to the conductivity. Specifically, the data are fit to the following equation:

$$T = (q/4 \times \pi \times k) \ln(t) + At + B, \quad (1)$$

where  $T$  is the temperature,  $q$  is the heat input to the sample per unit length of heat source per unit time, and  $k$  is the conductivity. In practice, the poorly conducting substrate absorbs a fraction of the heat during measurement, the amount of which depends on the ratio of sample to substrate conductivity. For most rock samples measured during Leg 148, this ratio was sufficiently large (>15–20) that the adjustment from the simple theory requires a relatively small correction. This correction was determined by carefully measuring materials whose conductivity was known and close to those measured in the samples.

Measurements of rock thermal conductivity by this technique were conducted sporadically during previous ODP legs. Measurements on 9 basalt samples were reported from Leg 109, Hole 648B (Shipboard Scientific Party, 1988b), as well as from Leg 111, Hole 504B (Shipboard Scientific Party, 1988a), and 38 gabbro samples from Leg 118, Hole 735B (Shipboard Scientific Party, 1989). These studies indicated that the multiplying factors used to convert the conductivity value calculated from the full-space theory to the actual value represented by the samples ranged from 2.1 to 2.7, depending on the time period used after initiation of the transient experiment. These factors were obtained by comparing well-established conductivity values for standard materials determined over the same time periods in the same apparatus.

Before measuring the samples obtained on Leg 148, calibration checks were performed using red and black rubber half-rounds and a slab of synthetic material designated as "macor" on each needle-probe. Measurements run over a transient needle-probe heating duration of 6 min suggested that the multiplying factors used to convert the conductivity values calculated from the full-space theory were best obtained during a time period between 60 and 240 s. Almost all the standard measurements produced the same heating pattern with an initially steep slope of temperature vs.  $\ln$  time over the first 60–90 s, gradually decreasing to a more uniform slope (Fig. 12). Most measurements of core samples from Leg 148 showed the same characteristics. To reduce the effects of any external temperature changes, all calibration runs were conducted when the temperature of the standard bath was changing at a rate less than 0.01°C/min.

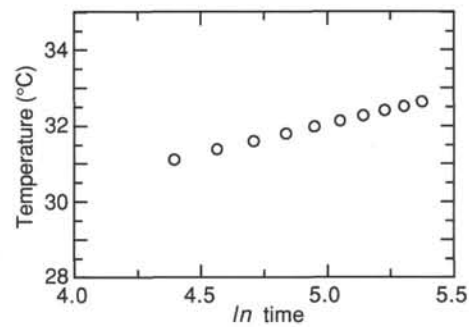


Figure 12. Typical plot of temperature vs. natural log ( $\ln$ ) time used for the calculation of the thermal conductivity values.

## Resistivity

During Leg 148, the electrical resistivity of hard rock samples from Hole 504B was measured at room temperature and atmospheric pressure, and an electrical current frequency of 50 Hz. This frequency was chosen because it is comparable to that used for downhole measurements with the Dual Laterolog (DDL). A two-electrode cell built aboard ship for hard rock samples and a Wayne-Kerr bridge were used to perform the measurements. The measurements were made on 25-mm diameter minicores kept saturated in seawater during the time period separating recovery on shipboard and the making of the measurements. The faces were cut smooth and parallel to allow good contact with the electrodes. To prevent a short circuit along the outer surface of the cylindrical minicore, each sample was wrapped in teflon tape prior to measurement. To prevent drying during the course of the measurement itself only small currents (on the order of 1  $\mu$ A) were used. Since the minicores are cylindrical in shape, the resistivity,  $R$ , of the samples is deduced from

$$r = R(L/S), \quad (2)$$

where  $r$  is the measured resistance,  $L$  is the length of the minicore, and  $S$  is the surface of the cross-section of the minicore.

## DOWNHOLE MEASUREMENTS

Downhole measurements are used to assess the physical, chemical, and structural properties of the formation surrounding the borehole. Interpretation of continuous logs and other discrete measurements can yield a stratigraphic, lithologic, structural, geophysical, and geochemical characterization of the hole. This information is especially important for holes such as Hole 504B that have poor core recovery. To log borehole data, sensors are lowered downhole on a seven-conductor cable, and each of several measuring devices continuously monitors the properties of the formation. Of the many different tool combinations available to ODP and in use in the petroleum industry, eight combinations of downhole sensors were planned for use on Leg 148: (1) a high-resolution temperature tool; (2) a Schlumberger geophysical combination; (3) a Schlumberger geochemical combination; (4) the Schlumberger formation microscanner (FMS); (5) a high-temperature digital borehole televiewer (BHTV); (6) a high-temperature, three-component magnetometer; (7) a triaxial geophone for a vertical seismic profile (VSP); and (8) a flowmeter and drillstring packer for permeability measurements.

As the leg developed, there were three exceptions to this planned program: (1) the BHTV failed; (2) the triaxial geophone did not function properly, so the VSP was conducted with a vertical-component Schlumberger geophone; and (3) the flowmeter was not deployed, by choice of the logging scientists. Brief descriptions of the downhole sensors and measurement procedures successfully used

during Leg 148 are given in this section. Refer to Hearst and Nelson (1984) and Ellis (1987) for more detailed descriptions of general logging principles and logging tools.

### Temperature Log

Borehole temperatures were logged shortly after the first Leg 148 reentry into Hole 504B prior to drilling, using a high-resolution tool designed for ODP at the Bureau de Recherche Géologiques et Minières (BRGM), France. The measurements were recorded at an average logging speed of 10 m/min from the seafloor to near the total depth of the hole, 2000.4 m. The temperature sensors are two accurately calibrated thermistors housed in a 5-mm-diameter tube located at the lower end of the probe. Temperatures were determined from the resistances of the two thermistors, which can be monitored separately or in combination for better sensitivity.

### Geophysical Combination

The Schlumberger geophysical combination used during Leg 148 consisted of the dual laterolog (DLL) to measure electrical resistivity and the array sonic tool (SDT) to measure acoustic wave velocities. This combination was used instead of the lithostratigraphic, or quad, combination more commonly run in ODP holes because it was better suited to the formation properties and scientific objectives of Leg 148.

The DLL provides two measurements of the formation electrical resistivity, labeled "deep" and "shallow" on the basis of respective horizontal depths of penetration of the current into the formation. The tool measures the intensity of a focused current flow from a downhole electrode to a remote return. The intensity of the measured current is inversely proportional to the formation resistivity. The tool design is such that the measurement remains accurate at the high resistivity values expected in crystalline rock. Measurement errors are <1% for formation resistivities up to 40,000  $\Omega\text{m}$ , and the vertical resolution is on the order of 0.6 m.

The measured resistivity is generally proportional to the inverse square root of porosity (Archie, 1942), so an apparent porosity profile can be constructed from the resistivity log. Other factors that may influence the formation resistivity include water salinity, clay content, temperature, concentration of hydrous and metallic minerals, the presence of vesicles, and the geometry of interconnected pore spaces. Also, in crystalline rock such as in Hole 504B, an estimate of the fracture porosity and orientation can be computed from comparison of the deep and shallow resistivity measurements (Pezard, 1990).

The SDT uses two acoustic transmitters and a series receivers to measure the time required for sonic waves to travel in the formation immediately surrounding the hole. The raw data are expressed as traveltimes for a sonic wave to pass through 0.31 m of formation; the data are then converted to sonic velocities. The vertical resolution of the tool is 0.61 m. Appropriate arrivals for the individual source-receiver paths are used to calculate the velocities of the different waves (e.g., compressional, shear, and surface waves) traveling in the formation. Only compressional wave velocities are determined aboard ship. The full sonic waveforms are recorded for post-cruise processing to determine shear-wave and Stoneley-wave velocities.

### Geochemical Combination

The Schlumberger geochemical combination consisted of a natural gamma-ray spectroscopy tool (NGT), an induced gamma-ray spectroscopy tool (GST), and an aluminum-clay tool (ACT). This tool combination measures the relative concentrations of 11 elements, including aluminum, silicon, calcium, iron, sulfur, titanium, hydrogen, chlorine, potassium, thorium, and uranium.

The NGT measures the natural radioactivity of the formation. Most of the detected gamma rays are emitted by the radioactive isotope  $^{40}\text{K}$  and radioactive isotopes of the U and Th decay series. The

gamma radiation originating in the formation close to the borehole is measured by a scintillation detector mounted inside the NGT sonde. Data analysis is conducted by dividing the entire incident gamma-ray spectrum into five discrete energy windows. At a given logging depth, the total counts recorded in each window are processed at the surface to give elemental abundances of K, U, and Th.

The GST induced gamma-ray device includes a pulsed source of 14-MeV neutrons and a gamma-ray scintillation detector. The GST employs prompt neutron capture, in which an atom captures a thermal neutron, becomes unstable and decays instantaneously, emitting gamma-rays. The raw gamma-ray spectrum is recorded and analyzed spectrally with a surface computer. The spectrum is dominated by characteristic sets of gamma rays from six elements: Ca, Si, Fe, Cl, H, and S. As their sum is always unity, the results do not reflect the actual elemental composition. Ratios of these elements are used in interpreting the lithology and porosity of the formation and the salinity of the formation fluid.

Aluminum abundance is determined with the ACT by neutron-induced gamma-ray spectroscopy using a  $^{252}\text{Cf}$  source. The contribution to the gamma-ray spectrum from natural radiation is removed by placing NaI gamma-ray detectors above and below the neutron source; when logging upwards, the upper detector measures the natural radiation before activation, and the lower detector measures the induced radiation after activation. It is then possible to subtract the naturally occurring component from the total measured after activation. Calibration to elemental weight percent (wt%) is performed by taking irradiated core samples of known volume, density, and composition and measuring their gamma-ray output when placed in a jig attached to the tool.

### FMS Electrical Imaging

The Schlumberger FMS is a microelectrical imaging device that allows for visual characterization of structures in the vicinity of the borehole wall from measurements related to the formation electrical conductivity (Ekstrom et al., 1986). The FMS string also includes the general purpose inclination tool (GPIT), which contains a three-component accelerometer and three-component magnetometer. The GPIT is used to measure the orientation of the downhole sensors within the borehole and the orientation (or deviation) of the borehole itself; in addition, it is used to compensate for instrument accelerations during FMS data acquisition.

The FMS produces high-resolution borehole images from electrical conductivity measurements made with closely spaced electrodes on four pads that are pressed against the borehole wall. The FMS used by ODP is a modified version of the standard Schlumberger FMS, with a slightly smaller diameter and 16 electrodes on each of the four pads. It has a vertical resolution of about 1 cm, but a detection threshold for conductive features on the order of microns. Raw data points are recorded every 2.5 mm, allowing detailed imaging of subsurface structures. This compares with conventional logs that are typically averaged over hundreds of mm; consequently, the sampling rate of the FMS is at least 100 times greater than most other logging tools.

The currents flowing among the FMS electrodes probe the conductivity of the rock to a depth of a few centimeters into the borehole wall, responding to variations in physical and chemical properties of the formation such as porosity or surface conduction in the presence of certain clay minerals. The conductivity traces are displayed side by side and then coded as an image in which black represents the most conductive values and white the most resistive values. The four images of 16 traces each are recorded simultaneously and processed at the conclusion of the log to allow on-site comparison with the cores. Possible applications of the FMS images include detailed correlation of coring and logging depth, orientation of cores, identification and mapping of fractures, faults, and foliations, and determination of strike and dip of imaged structures (Pezard and Luthi, 1988). In addition it may be possible to determine in-situ horizontal stress orientation from FMS calipers in breakouts, as described below for the BHTV.

## Magnetometer

Downhole magnetic measurements were conducted with a high-temperature, three-component magnetometer recently developed by the Bundesanstalt für Geowissenschaften und Rohstoffe (BGR) in Germany. It contains three orthogonally oriented fluxgate sensors (made by IFG, Canada) that can measure fields up to 100  $\mu\text{T}$  with a resolution of 0.1 nT. The probe also contains two inclinometers aligned with the probe's horizontal  $x$ - and  $y$ -axes that are used to measure the tilt of the probe to 0.1°. For azimuthal orientation, the probe had been designed to contain a gyro, but the manufacturer did not deliver the gyro in time for Leg 148. Data are transmitted at a sampling interval of 0.5 s from the three fluxgates and two inclinometers; internal temperature and voltage are also monitored. The high-temperature capabilities of the system have been achieved by insulation with a non-magnetic steel dewar, including two heat sinks, and use of low power electronics with a maximum working temperature of 125°C. The tool has been tested to withstand internal temperatures < 125°C for up to 54 hr in an external environment held at 160°C. Calculations indicate that the magnetometer should work for up to 10 hr at an external temperature of 300°C. Prior to Leg 148, the magnetometer was successfully operated in the KTB (Kontinentales Tiefbohrprogramm Bundesrepublik, or German Continental Deep Drilling Program) main hole to a depth of 6000 m with a bottom-hole temperature of 170°C.

## Vertical Seismic Profile

A vertical seismic profile (VSP) entails clamping a geophone or seismometer to the borehole wall at different depths and recording the seismic wavefield generated from a source at the surface vertically above the seismometer. This technique provides the intermediate mapping linkage between reflection profiles used for regional surveying and the lithology and structure determined from cores and logs from the borehole (e.g., Mutter and Balch, 1988). A VSP involves measurement of both seismic transmission and reflection; its aperture is typically much smaller than that found in surface reflection profiles. The seismometer records both the direct, downgoing waves as well as upgoing waves reflected from acoustic impedance changes in the formation below the clamping depths. Detailed interval velocities between clamping depths can be calculated from differences in the arrival times of the direct waves. Analyses of the measured wavefields are used for correlation with subsurface stratigraphic relationships, lithological conditions, and physical properties determined from the recovered cores and other geophysical logs. The data can also be used to estimate the acoustic properties and depths to interfaces below the total depth of the hole.

The seismometer planned to be used for the Leg 148 experiment is a three-component Geospace tool provided by the Woods Hole Oceanographic Institution (WHOI) and upgraded for the temperatures of about 200°C anticipated at the bottom of Hole 504B. When this tool failed to perform properly, the experiment was instead conducted with a Schlumberger vertical-component seismometer. Two separate sound sources were used: a 400-in.<sup>3</sup> water gun (SSI Model S400) and a 300-in.<sup>3</sup> air gun (Bolt Model PAR 1500), both operated with air pressure of about 1900 psi. The seismometer is clamped to the borehole wall using an arm that is activated from the ship, and the guns are shot successively until the desired number (5–10) of signals of acceptable quality have been recorded from each source. The tool is then unclamped and moved to the next clamping position, where the sequence is repeated.

A VSP was conducted through the upper 1535 m of Hole 504B during Leg 111, using a vertical-component Schlumberger tool at 10-m intervals (Shipboard Scientific Party, 1988a). The Leg 148 experiment was planned to use the same clamping interval, primarily in the deeper section of the hole drilled subsequent to the Leg 111 experi-

ment. Before running the VSP, experiments were conducted to calibrate the source signature, to review optimal source depths, and to facilitate integration of the Leg 148 data with the Leg 111 data. These are described in the "Site 504" chapter (this volume), as is a more detailed narrative of the experiment and data-processing techniques.

## Packer Experiments

Formation permeabilities were measured using a resettable drill-string packer manufactured by TAM International and described by Becker (1986, 1988). This packer incorporates inflatable rubber elements to isolate a section of the hole and can be configured as a single or a straddle packer. For the measurements during Leg 148 it was configured with two elements and used as a single-seal packer to hydraulically isolate the zone between the bottom of the hole and the seal. Once the packer was inflated, two kinds of experiments were used to determine the average permeability of the isolated interval: standard pressure pulse, or "slug" tests, and constant-rate injection tests.

The slug tests were conducted following procedures described by Cooper et al. (1967), Papadopoulos et al. (1973), Bredehoeft and Papadopoulos (1980), and Neuzil (1982), and the injection tests were conducted using methods described by Papadopoulos, Horner (1951), and Mathews and Russell (1967). When used for such measurements, the packer is actuated using a "go-devil" that is dropped down the drill string into the packer inflation subassembly. The go-devil also carries recorders to monitor downhole fluid pressures in the isolated, pressurized zone during the experiment; these pressures are the primary data from which permeability is calculated. Two types of pressure recorders were used during Leg 148: mechanical "K-3" gauges made by Kuster Company, and electronic "ERPG-300" gauges made by Geophysical Research Corporation. The K-3 gauges record analog pressure mechanically by scratching a metal chart; the ERPG-300 gauges record in electronic memory 10000 digital pressure values sampled at 8.64 s intervals over 1 day. The entire drill string, as well as the isolated zone, was pressurized during testing, and a pressure transducer at the rig floor was also used to provide a real-time indication of downhole events. Pumping rates and total volumes pumped were also measured at the rig floor.

## Quality and Analysis of Logging Data

The quality of downhole logging data may be seriously degraded in sections of the borehole that have large diameters or rapid changes in the hole diameter. Electrical resistivity measured with the DLL is least sensitive to such borehole effects. The nuclear measurements (density, neutron porosity, and both natural and induced spectral gamma rays) are most seriously impaired because of the large attenuation by the borehole fluid. Corrections can be applied to the original data to reduce the effects of these conditions. Different logs may have small depth mismatches caused by cable stretch or ship heave during recording. Small errors in depth matching can also impair the results in zones of rapidly varying lithology. To minimize such errors, a hydraulic heave compensator adjusts for ship motion in real time. Downhole data cannot be precisely matched with core data in zones where core recovery is low because of the inherently ambiguous placement of the recovered section within the interval cored.

Throughout the acquisition of downhole measurements, incoming data are observed in real time on a monitor oscilloscope and simultaneously recorded on digital tape. After the completion of a set of downhole measurements tapes are formatted to allow for shipboard analysis. The precise nature of the analysis procedure varies for each site. Although initial appraisal of the downhole data is carried out aboard ship, further analyses are undertaken after the end of the leg. Post-cruise analyses include standardization of a depth reference, re-processing of acoustic logs using full waveform data, processing of BHTV and FMS images to analyze structures in the formation and to

determine the stress field from breakouts, and reprocessing of geochemical log data to estimate absolute elemental weight percentages and mineralogy (e.g., Herzog et al., 1987; Harvey et al., 1991).

## REFERENCES\*

- Archie, G.E., 1942. The electrical resistivity log as an aid in determining some reservoir characteristics. *J. Pet. Tech.*, 5:1-8.
- Becker, K., 1986. Special report: development and use of packers in ODP. *JOIDES J.*, 12:51-57.
- , 1988. A guide to ODP tools for downhole measurements. *ODP Tech. Notes*, 10.
- Becker, K., Foss, G., et al., 1992. *Proc. ODP, Init. Repts.*, 137: College Station, TX (Ocean Drilling Program).
- Boyce, R.E., 1976. Definitions and laboratory techniques of compressional sound velocity parameters and wet-water content, wet-bulk density, and porosity parameters by gravimetric and gamma ray attenuation techniques. In Schlanger, S.O., Jackson, E.D., et al., *Init. Repts. DSDP*, 33: Washington (U.S. Govt. Printing Office), 931-958.
- Bredehoeft, J.D., and Papadopoulos, S.S., 1980. A method for determining the hydraulic properties of tight formations. *Water Resour. Res.*, 16:223-238.
- Brewer, T.S., 1985. Geochemistry, geochronology and tectonic setting of the Proterozoic Telemark supracrustals, southern Norway [Ph.D. thesis]. Univ. of Nottingham.
- Clanton, U.S., and Fletcher, C.R., 1976. Sample size and sampling errors as the source of dispersion in chemical analyses. *Proc. Lunar Sci. Conf.*, 7:1413-1428.
- Cooper, H.H., Jr., Bredehoeft, J.D., and Papadopoulos, I.S., 1967. Response of a finite diameter well to an instantaneous charge of water. *Water Resour. Res.*, 3:267-269.
- Cox, S.F., and Etheridge, M.A., 1983. Crack-seal fibre growth mechanisms and their significance in the development of oriented layer silicate microstructures. *Tectonophysics*, 92:147-170.
- Dick, H.J.B., Erzinger, J., Stokking, L.B., et al., 1992. *Proc. ODP, Init. Repts.*, 140: College Station, TX (Ocean Drilling Program).
- Dick, H.J.B., Meyer, P.S., Bloomer, S., Kirby, S., Stakes, D., and Mawer, C., 1991. Lithostratigraphic evolution of an in-situ section of oceanic Layer 3. In Von Herzen, R.P., Robinson, P.T., et al., *Proc. ODP, Sci. Results*, 118: College Station, TX (Ocean Drilling Program), 439-540.
- Ekstrom, M.P., Dahan, C.A., Chen, M.-Y., Lloyd, P.M., and Rossi, D.J., 1986. Formation imaging with microelectrical scanning arrays. *Trans. SPWLA 27th Ann. Logging Symp.*, Pap. BB.
- Ellis, D.V., 1987. *Well Logging For Earth Scientists*: New York (Elsevier).
- Gieskes, J.M., and Peretsman, G., 1986. Procedures of interstitial water analysis. *ODP Tech. Note*, 5.
- Harvey, P.K., and Atkin, B.P., 1983. Automated X-ray fluorescence analysis. In *Sampling and Analysis for the Minerals Industry*. Inst. Min. Metall.
- Harvey, P.K., Lovell, M.A., and Bristow, J.F., 1991. The interpretation of geochemical logs from the oceanic basement: mineral modeling in ODP Hole 735B. *Nucl. Geophys.*, 5:267-277.
- Harvey, P.K., Taylor, D.M., Hendry, R.D., and Bancroft, F., 1973. An accurate method for the analysis of rocks and chemically related materials by X-ray fluorescence spectrometry. *J. X-Ray Spectrom.*, 2:33-44.
- Hearst, J.R., and Nelson, P.H., 1984. *Well Logging for Physical Properties*: New York (McGraw-Hill).
- Herzog, R., Colson, L., Seeman, B., O'Brien, M., Scott, H., McKeon, D., Wright, P., Grau, J., Ellis, D., Schweitzer, J., and Herron, M., 1987. Geochemical logging and spectrometry tools. *Soc. Pet. Eng., Spec. Pap.*, 16792:447-460.
- Horner, D.R., 1951. Pressure build-up in wells. *Proc. Third World Pet. Congr.*, 2:501.
- Jaeger, J.C., 1956. Conduction of heat in an infinite region bounded internally by a circular cylinder of a perfect conductor. *Aust. J. Phys.*, 9:167-179.
- MacKenzie, W.S., Donaldson, C.H., and Guilford, C., 1982. *Atlas of Igneous Rocks and Their Textures*: New York (Wiley).
- Mathews, C.S., and Russell, D.G., 1967. *Pressure Build-up and Flow Tests in Wells*. Soc. Pet. Eng., AIME, Monogr. 1.
- Munsell Soil Color Charts, 1971. Baltimore, MD (Munsell Color).
- Mutter, J.C., and Balch, A., 1988. *Vertical Seismic Profiling (VSP) and the Ocean Drilling Program (ODP): Report of a Workshop*. Joint Oceanogr. Inst./U.S. Science Advisory Comm.
- Neuzil, C.E., 1982. On conducting the modified "slug" test in tight formations. *Water Resour. Res.*, 18:439-441.
- Norrish, K., and Chappell, B., 1977. X-ray fluorescence spectrometry. In Zussman, J. (Ed.), *Physical Methods in Determinative Mineralogy*: New York (Academic Press), 201-272.
- Norrish, K., and Chappell, B.W., 1967. X-ray spectrography. In Zussman, J. (Ed.), *Physical Methods in Determinative Mineralogy*: New York (Academic Press), 161-124.
- Papadopoulos, S.S., Bredehoeft, J.D., and Cooper, H.H., 1973. On the analysis of "slug test" data. *Water Resour. Res.*, 9:1087-1089.
- Petit, J.P., 1987. Criteria for the sense of movement on fault surfaces in brittle rocks. *J. Struct. Geol.*, 9:597-608.
- Pezard, P.A., 1990. Electrical properties of mid-ocean ridge basalt and implications for the structure of the upper oceanic crust in Hole 504B. *J. Geophys. Res.*, 95:9237-9264.
- Pezard, P.A., and Luthi, S.M., 1988. Borehole electrical images in the basement of the Cajon Pass Scientific Drillhole, California; fracture identification and tectonic implications. *Geophys. Res. Lett.*, 15:1017-1020.
- Potter, D.K., and Stephenson, A., 1990. Field-impressed anisotropies of magnetic susceptibility and remanence in minerals. *J. Geophys. Res.*, 95:15573-15588.
- Robinson, P.T., Von Herzen, R., et al., 1989. *Proc. ODP, Init. Repts.*, 118: College Station, TX (Ocean Drilling Program).
- Shipboard Scientific Party, 1988a. Site 504: Costa Rica Rift. In Becker, K., Sakai, H., et al., *Proc. ODP, Init. Repts.*, 111: College Station, TX (Ocean Drilling Program), 35-251.
- , 1988b. Site 648. In Detrick, R., Honnorez, J., et al., *Proc. ODP, Init. Repts.*, 106/109: College Station, TX (Ocean Drilling Program), 35-134.
- , 1989. Site 735. In Robinson, P.T., Von Herzen, R., et al., *Proc. ODP, Init. Repts.*, 118: College Station, TX (Ocean Drilling Program), 89-222.
- Sibson, R.H., 1977. Fault rocks and fault mechanisms. *J. Geol. Soc. London*, 133:191-214.
- Staudigel, H., 1979. Chemical analyses of inter-laboratory standards. In Donnelly, T., Francheteau, J., Bryan, W., Robinson, P., Flower, M., Salisbury, M., et al., *Init. Repts. DSDP*, 51, 52, 53: Washington (U.S. Govt. Printing Office), 1331-1333.
- Thompson, G., and Bankston, D.C., 1970. Sample contamination from grinding and sieving determined by emission spectroscopy. *Appl. Spectros.*, 24:210-219.
- Vacquier, V., 1985. The measurement of thermal conductivity of solids with a transient linear heat source on the plane surface of a poorly conducting body. *Earth Planet. Sci. Lett.*, 74:275-279.
- Von Herzen, R.P., and Maxwell, A.E., 1959. The measurement of thermal conductivity of deep-sea sediments by a needle-probe method. *J. Geophys. Res.*, 64:1557-1563.

\* Abbreviations for names of organizations and publications in ODP reference lists follow the style given in *Chemical Abstracts Service Source Index* (published by American Chemical Society).